nature communications

Article

https://doi.org/10.1038/s41467-024-54494-6

miR394 and LCR cooperate with TPL to regulate AM initiation

Received: 15 April 2024

Accepted: 9 November 2024

Published online: 23 November 2024

Check for updates

Liya Liu[1,2], Binbin Hu[1,2], Siying Guo[1,2], Zhihui Xue[1], Tao Wang[1] & Cui Zhang[1]

Plant architecture is a main determinate of crop yield, and lateral branching significantly influences the number of inflorescences and seeds. The mechanism of axillary bud initiation remains unclear. This work aimed to examine how miRNAs regulate axillary bud initiation. By constructing a small RNA library and screening a mutant population, we revealed the initiation of axillary buds is specifically induced by miR394 and repressed by its target, *LEAF CURLING RESPONSIVENESS* (*LCR*). Using promoter-driven fluorescent tags and in situ hybridization, we showed that miR394 is localized in the center of the leaf axil where AMs are initiated. Through molecular and genetic research, we revealed that miR394/*LCR* may regulate *REVOLUTA* (*REV*) and *SHOOT MERISTEMLESS* (*STM*) to establish the axillary meristem. Immunoprecipitation-mass spectrometry studies revealed that LCR, as an F-box protein, may interact with TOPLESS (TPL) proteins and participate in ubiquitinated protein degradation. Our results reveal an important mechanism by which the miR394-regulated LCR accelerates the degradation of TPL to precisely modulate axillary bud initiation.

The axillary meristem (AM) is a highly dynamic and continuously active stem cell system located in leaf axils and is responsible for the generation of lateral shoots in plants[1–3]. AM development includes initiation and bud outgrowth[4]. During AM initiation, a morphologically detectable bump emerges from the axils of leaves and develops into a bud[5,6]. Little is known about AM initiation due to its subtle structure. To date, several transcription factors (TFs) that regulate AM initiation have been characterized[6–14].

As AMs initiate at the boundaries between the SAM and young leaf primordia, some transcription factors, including *CUP SHAPED COTYLEDON* (*CUCs*)[9], *LATERAL SUPPRESSOR* (*LAS*)[8] and *REGULATOR OF AXILLARY MERISTEMS* (*RAXs*)[13], enriched in the boundaries specify boundary formation and affect AM initiation. AM initiation requires a meristematic cell population that continuously expresses the marker gene *STM*[6,10,14]. *STM* expression is dynamic and associated with two phases of stem cell division. In the first phase, in leaf axils younger than P_9 (the ninth earliest leaf primordium), *STM* is expressed at a low level that is sufficient for stem cell competence but not for AM initiation[10]. In the second phase, *STM* is highly expressed in leaf axils older than P_{10}, which promotes the formation of AMs[10]. *REV*, which belongs to the HD-ZIPIII family targeted by miR165/166, is expressed co-ordinately with AM initiation and is the only member of this family that can activate stem cells during AM initiation[5,15,16]. The level of *REV* is kept low on the adaxial side of young leaf axils (<P_{10}) and increases in the old leaf axils (>P_{11}) when AMs initiate[14,17]. REV was found to promote *STM* directly by binding the *STM* promoter to activate AM initiation[10]. After the induction of *STM* and gain of meristem activity, the homeodomain transcription factor *WUSCHEL* (*WUS*) promotes AM initiation around P_{13} leaf axils[11]. *WUS* expression is also feedback regulated by *CLAVATA3* (*CLV3*) in AMs[12]. Auxin and cytokinins are two major hormones that regulate meristem development[18]. In boundaries and AMs, these two hormones, along with brassinosteroids (BRs), also play vital roles[11,17,19,20]. In some cases, TFs in these hormonal pathways combine with general transcription repressors, such as *TPL*, to precisely regulate meristem marker genes[21–25].

MicroRNAs (miRNAs), endogenous small noncoding RNAs ranging in length from 20 to 24 nucleotides, play critical roles in plant development[26–31]. miRNAs control target gene expression at the

[1]Key Laboratory of Plant Molecular Physiology, Institute of Botany, Chinese Academy of Sciences, Beijing 100093, China. [2]University of Chinese Academy of Sciences, Beijing 100049, China. e-mail: cuizhang@ibcas.ac.cn

posttranscriptional level by directly cleaving target mRNAs or inhibiting their translation[32,33]. Although the ability of miR165/166 to cleave *REV* and the role of the miRNA effector *ARGONAUTE10* (*AGO10*) in AM initiation have been reported[17,34,35], whether other miRNAs participate in AM development and how they function are unknown.

miR394 is a highly conserved miRNA of 20 nucleotides that was first identified in *Arabidopsis thaliana*[36,37]. Previous studies have reported that miR394 is involved in regulating meristem development, leaf morphogenesis, and stress resistance pathways[38–45]. In the shoot apical meristem, miR394 acts as a mobile signal produced from the protoderm and moves to the underlying cells to maintain stem cell activity by balancing the loop of *WUS-CLV3*. In its destination, the organizing centre (OC), miR394b inhibits the transcript levels of its target *Leaf Curling Responsiveness* (*LCR*)[39]. Furthermore, LCR may associate with the MLP-LIKE PROTEIN 28 (MLP28) family member to regulate SAM development[41]. However, the involvement of miR394 and *LCR* in AM development has not been reported, and the pathways affected by miRNAs and F-box proteins remain intriguing.

In this study, we constructed a small RNA library using boundary enrichment tissues, screened miRNAs potentially involved in AM development, and discovered that miR394 was highly expressed in AMs. We found that miR394/LCR expression exhibited temporal and spatial patterns that closely matched the dynamics of AM initiation: miR394 inhibited *LCR* in the adjacent domain between the leaf adaxial side and boundary, where AMs initiate. The inhibition continued throughout AM initiation within the buds. Moreover, we found that *LCR* down-regulated *STM* and *REV* expression. In addition, LCR acts as a specific Skp1/Cullin1/F-box (SCF) E3 ligase complex and targets *TPL*, which functions as a positive regulator of AM initiation. Collectively, our findings identified three modulators of AM initiation and established a pathway mediated by miR394 and F-box proteins in AMs.

Results

miR394 promoted and *LCR* inhibited AM initiation in *Arabidopsis*

To identify miRNAs involved in axillary meristem formation, we sampled seedlings from Col-0 plants grown under short-day conditions for 10 days (had only 2–4 leaves and almost no AMs had formed) and boundary enrichment tissues (vegetative shoot apex with leaf removal) from Col-0 plants grown under short-day conditions for 30 days (approximately 26 to 30 leaves emerged, at which time a large number of AMs were initiated in leaf axils), individually. Small RNA sequencing (sRNA-seq) were used to profile miRNA expression and we compared the sRNA-seq data of the vegetative shoot apex with that of the seedlings. Ultimately, we identified 46 up-regulated and 39 down-regulated high-confidence differentially expressed (DE) miRNAs (FDR < 0.5) (Supplementary Data 1). It was worth noting that among these DE miRNAs, miR394a and miR394b were highly enriched with great significance at the boundaries (Fig. 1a). Previous studies have shown that *mir394b-1* produces "pin-like" shoots in the *ago10-1* background, which is indicative of stem cell defects in *Arabidopsis*[39,46]. By screening a small RNA-related mutant population, we confirmed that AMs consistently failed to form in many rosette leaf axils of *mir394b-1* but normally formed in every leaf axil of the wild type (Fig. 1b). To understand how miR394 regulates the formation of AMs in rosette leaf axils in more detail, we knocked out *miR394a* and *miR394b* via CRISPR/Cas9 in *mir394a-cr* and *mir394b-cr* lines and overexpressed *miR394a* and *miR394b* in *miR394A-OX* and *miR394B-OX* lines (Supplementary Fig. 1a–c). After genomic identification, three independent homozygous lines for each genotype were selected for further study (Supplementary Fig. 1d–f). We found that both the *mir394a-cr* lines (#1 delete 1 bp, #2 delete 44 bp and #3 delete 45 bp) and the *mir394b-cr* lines (#1 delete 2 bp, #2 delete 28 bp and #3 add 1 bp) presented AM defects similar to but less severe than those of *mir394b-1* (Fig. 1b and Supplementary Fig. 2a). We further quantified AMs of the *mir394a/b* double mutant and observed many fewer AMs than in the single mutants (Fig. 1b, c), suggesting that miR394a and miR394b may act redundantly in controlling AM formation. In contrast, compared with the WT, *miR394-OX* did not result in a change in the number of AMs (Supplementary Fig. 2a).

To determine whether *LCR* gene, which is a known miR394 targets, is the cause of AM defects[36], quantitative real-time PCR (qRT-PCR) was used to measure *LCR* mRNA in the miR394 mutants. *LCR* was expressed at much higher levels when miR394a and miR394b were knocked down in the *mir394a/b* double mutant (Supplementary Fig. 1d, e). To analyze whether *LCR* inhibits AM formation, we obtained a loss-of-function mutant of *LCR*, *lcr-1* (SALK_136833), with a T-DNA insertion and generated *lcr*-cr lines via CRISPR/Cas9 (Supplementary Fig. 3a, b). After PCR confirmation, we obtained three independent homozygous *lcr-cr* mutants (#1 delete 6 bp, #2 delete 21 bp and #3 add 1 bp) for further study. Both the *lcr-1* and *lcr-cr* mutants presented reduced *LCR* mRNA levels (Supplementary Fig. 3c, d) and normal AM formation (Supplementary Fig. 2a). Moreover, we expressed *LCR* and the miR394-resistant versions *LCR4m*[39] and *LCR5m*[43] in Col-0, driven by the *LCR* promoter or the CaMV *35S* promoter (Supplementary Fig. 4a). Genotyping combined with qRT-PCR and immunoblot analyses confirmed that we had obtained more than three independent *LCR-OX* and *LCR4m-OX* homozygous lines (Supplementary Fig. 4b–e). As expected for the miR394 targets, *LCR* mRNAs were highly accumulated in *pLCR::LCR4m* and *p35S::LCR4m* (Supplementary Fig. 4c), leading to a strong AM deficiency phenotype (Fig. 1b, c). We carefully analyzed AM development in *p35S::LCR4m*, whose phenotype was more severe, and found that 97.7% of rosette leaves presented bare axils. Among cauline leaf axils, 71.4% were without AMs, 14.3% had terminated buds, and 14.3% had filamentous structures. In addition, *p35S::LCR4m* also presented defects in floral primordia (Supplementary Fig. 5a–o). In contrast to the *LCR4m-OX* plants, *LCR* loss-of-function mutants grew faster and formed normal AMs in rosette leaves (Supplementary Fig. 2a). Notably, the AM defect of *mir394a/b* was rescued by crossing with *lcr-1* (Supplementary Fig. 2a), confirming that miR394 promotes AM formation through the downregulation of *LCR* mRNA.

We observed the AM morphology of the *mir394a/b* double mutant, *pLCR::LCR4m*, *p35S::LCR4m* and WT via scanning electron microscopy (SEM). While the WT had obvious dome-shaped bulges at the adaxial base of P_{15}, the *mir394a/b* double mutant, *pLCR::LCR4m* and *p35S::LCR4m* lacked proliferating cells at the leaf axils at the same stage (Fig. 1d). We observed anatomical changes in the leaf axils through tissue sectioning. In the WT, more densely stained cells formed morphologically distinguishable bumps at stages P_{14} to P_{16}. In the *mir394a/b* double mutant, *pLCR::LCR4m* and *p35S::LCR4m*, the frequencies of densely stained cells and AM structures were highly reduced in the leaf axils at the same stages (Fig. 1e). Taken together, these data indicate that miR394 expression in the leaf axil is necessary for AM initiation.

LCR encodes a conserved F-box protein[47–49] (Supplementary Fig. 6a–d and Supplementary Data 2). To confirm whether LCR affects AM initiation through the F-box domain, we constructed overexpression lines in which the F-box domain was removed (Supplementary Fig. 4a–e). We tracked AM development in $LCR^{\Delta F\text{-}box}$-*OX* and $LCR4m^{\Delta F\text{-}box}$-*OX* plants and found that most leaf axils formed normal AMs (Supplementary Fig. 2a–e). These results indicate that *LCR* may act as a negative regulator of AM initiation through its F-box domain.

miR394 and LCR are expressed on the adaxial side of leaves and AMs

AMs are initiated at the boundary zone in the shoot apex during vegetative development. AM initiation is regulated temporally and spatially, and a morphologically distinguishable structure is formed by P_{11}. We therefore tested whether miR394 is expressed in the shoot apex. To visualize the real-time dynamics of miR394 expression, we constructed *pMIR394A::GFPer* and *pMIR394B::GFPer* reporter lines

https://doi.org/10.1038/s41467-024-54494-6

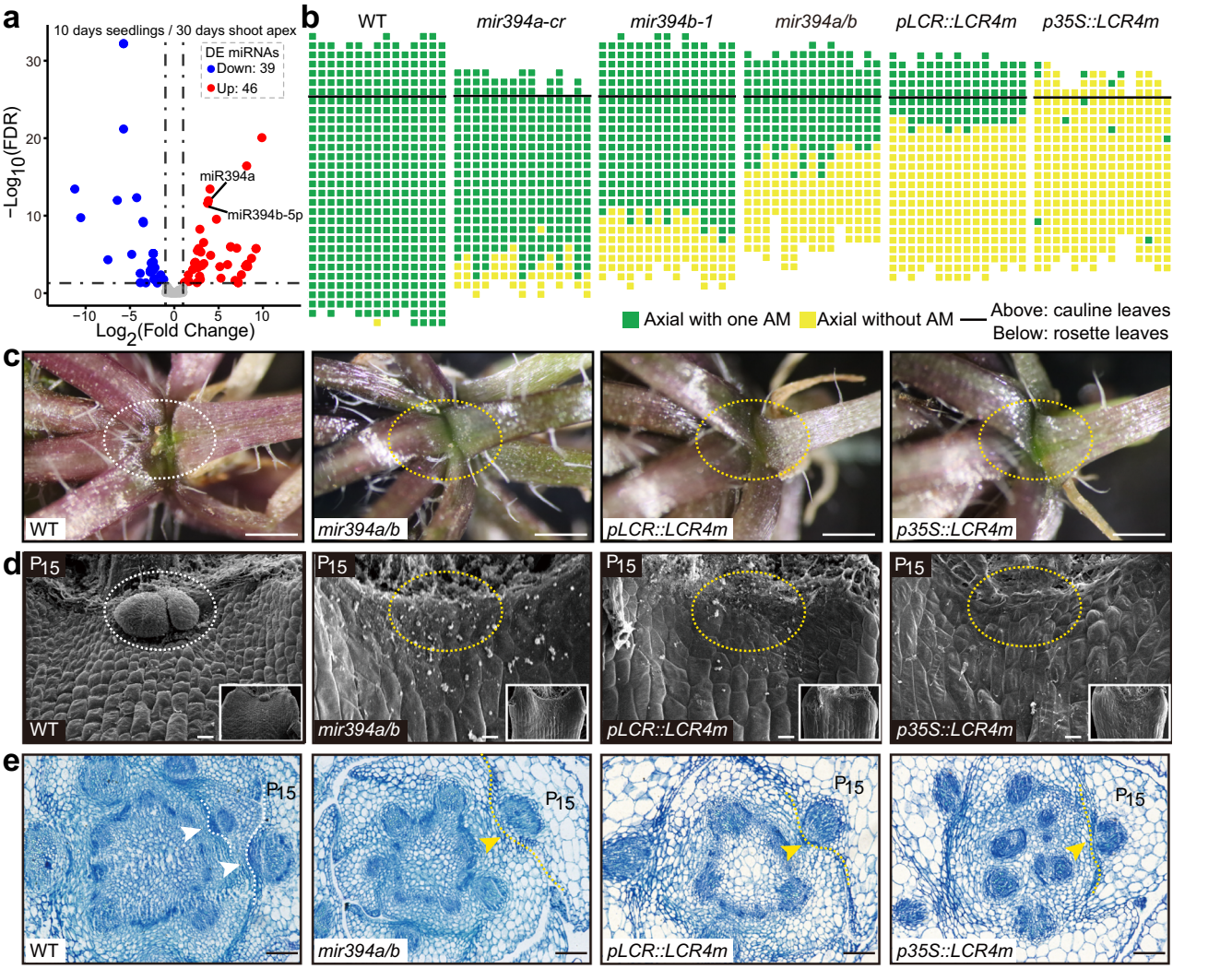

Fig. 1 | miR394 controls axillary bud formation. a Volcano plots showing differentially expressed (DE) miRNAs in SAMs and AMs compared with whole seedlings determined by sRNA-seq. The red dots represent miRNAs whose expression was significantly up-regulated, the blue dots represent miRNAs whose expression was significantly down-regulated, and the gray dots represent miRNAs whose expression was not significantly changed. **b** Schematic representation of axillary bud formation. Compared with the WT, the *mir394a-cr*, *mir394b-1*, *mir394a/b* double mutant, *pLCR::LCR4m* and *p35S::LCR4m* transgenic lines presented different degrees of AM defects in early leaves. The thick black horizontal line represents the border between the youngest rosette leaf and the oldest cauline leaf. Each column represents a single plant, and each square represents an individual leaf axil. The bottom row represents the oldest rosette leaf axils, with progressively younger leaves above. Green indicates the presence of an axillary bud; yellow indicates the absence of an axillary bud. All the plants were grown under short-day conditions for 30 days and then shifted to long-day conditions for 30 days to count the number of axillary buds. **c** Morphology of rosette leaf axils in WT, *mir394a/b* mutant, *pLCR::LCR4m* or *p35S::LCR4m* transgenic lines. AM was visible in the WT (white dotted circle) but absent in the other genotypes (yellow dotted circle) under a dissecting microscope. All the plants were grown under short-day conditions for 30 days and then subjected to long-day conditions for 30 days. Scale bars, 1 mm. **d** Scanning electron micrographs of the basal regions of P_{15} rosette leaves showing AM formation (white dotted circle) in WT but the absence of AMs (yellow dotted circle) in the *mir394a/b* mutant or *LCR4m* overexpression lines. The plants were grown under short-day conditions for 21 days. Scale bars, 20 μm. **e** Cross sections of vegetative shoot apex were stained with toluidine blue O. Images show a dome-shaped AM in the leaf axil of P_{15} in WT (arrows) but not in the *mir394a/b* mutant or *LCR* overexpression lines (yellow arrows). The plants were grown under short-day conditions for 30 days. Scale bars, 100 μm. At least three samples were analyzed with similar results for each experiment in (**c**–**e**).

(Supplementary Fig. 7a, b) and tracked miR394 transcription in young leaf axils. We found that *MIR394A* had a strong signal in the boundary region between the emerging leaf primordia and the SAM, and this signal spread into the adaxial domain of the leaves as well but was lower in AMs (Fig. 2a and Supplementary Fig. 8a). In addition, a similar pattern of *MIR394B* expression was observed in primordia and boundary cells as that of *MIR394A*, but the signals in AMs were relatively greater than those in *MIR394A* (Fig. 2b and Supplementary Fig. 8b). RNA in situ hybridization assays revealed that mature miR394 accumulated in the SAM, AMs, vasculature, and leaf primordia (especially the adaxial domain) (Fig. 2c). Through tracking of miR394 at boundaries and AMs, we found that miR394 was enriched in the upper cell layers and the center of the leaf axils where AMs initiate (phase 1–2) and was continuously expressed throughout the initiation of AMs (phase 3–9) (Supplementary Fig. 9a–p). These results indicated that miR394a and miR394b were co-expressed at the boundary but partially overlapped in AMs, implying the overlapping and distinguishing roles of the family members.

To investigate the expression patterns of *LCR* during AM initiation, we constructed LCR and LCR4m reporters by fusing the CDS to GFP under the native *LCR* promoter, but no stable LCR signal was captured, even with F-box removal. Therefore, referring to a previous report[39], we amplified a fragment containing the *LCR* promoter, the first exon, and three amino acids from the second exon and fused it to

https://doi.org/10.1038/s41467-024-54494-6

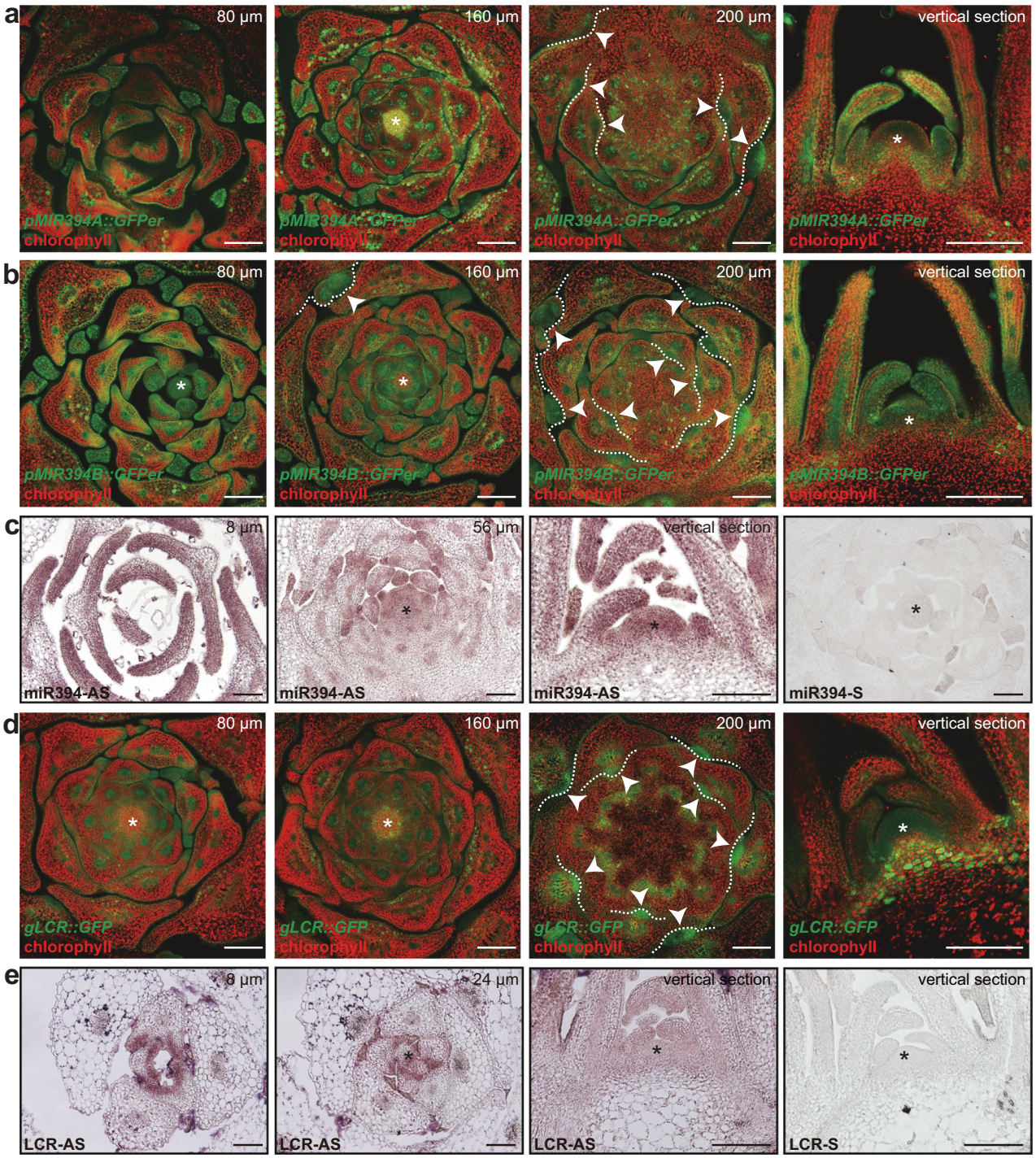

Fig. 2 | miR394 and LCR are expressed on the adaxial side of leaves and AMs. **a**, **b** Longitudinal and transverse sections through the vegetative shoot apex of *pMIR394A::GFPer* and *pMIR394B::GFPer*. *MIR394A* (**a**) and *MIR394B* (**b**) signals are shown in green, and the autofluorescence of chlorophyll is shown in red. **c** In situ hybridization revealed the expression patterns of mature miR394. **d** Expression of *LCR* (green) in the shoot apex. Sections were mix with autofluorescence (red). **e** *LCR* mRNA accumulation in the shoot apex was determined via RNA in situ hybridization in *pLCR::LCR4m*. Confocal images were taken of agarose sections. The asterisks represent the SAM, the arrows represent AMs, and the dashed lines represent the leaf axils where AMs were initiated. The numbers in the upper right corner represent the relative distances from the shoot apex. All the plants were grown under short-day conditions for 30 days. AS, antisense probes; S, sense probes. Scale bars, 100 μm. At least three samples were analyzed with similar results for each experiment in (**a**–**e**).

GFP to form an miR394-resistant transcriptional reporter of *gLCR::GFP* (Supplementary Fig. 7a, b). Using this reporter line, we found that GFP was strongly enriched in the adaxial domain of leaf primordia, boundaries, SAM and AMs (Fig. 2d and Supplementary Fig. 8c). In addition, although endogenous and exogenous LCR was not detected in *pLCR::LCR* via in situ hybridization, the miR394-resistant version of *pLCR::LCR4m* presented a similar mRNA distribution in leaf axils to that of the *gLCR::GFP* reporter (Fig. 2e), suggesting that miR394 inhibits *LCR* post transcriptionally in leaf axils.

To further confirm the role of the LCR protein in leaf axils, we specifically expressed *LCR5m*, driven by the abaxial domain-specific promoter *KANADI* (*KAN1*) or the adaxial domain-specific promoter *REV*

(Supplementary Fig. 7a, b). We found that *pREV::LCR4m* presented a phenotype similar to that of *pLCR::LCR4m*, with severe defects in AMs, but that of *pKAN1::LCR4m* remained the same as that of the WT (Supplementary Fig. 10a–c). It is known that miR394 inhibits *LCR* transcript levels, but it remains to be determined whether miR394 inhibition of *LCR* is required for AMs initiation (Fig. 2 and Supplementary Fig. 11a–d). Transgenic plants harboring *p35S::LCR-GFP* and *p35S::LCR4m-GFP* were obtained, and nuclear signals were verified in the root tips (Supplementary Fig. 11e, i). While strong LCR4m signals were observed in the shoot apex, only a weak LCR signal was captured in cells below the SAM (Supplementary Fig. 11f–h, j–l). Moreover, western blot analysis confirmed that the LCR4m protein was significantly more highly expressed than the LCR protein (Supplementary Fig. 11q, r), confirming that the expression of *LCR* was strictly controlled by miR394 in the shoot apex. In addition, after removing the F-box domain, $LCR^{\Delta F\text{-box}}$ still presented similar signals in root nuclei as the full-length protein (Supplementary Fig. 11m), and a weak signal appeared in the adaxial domain of the leaves and AMs (Supplementary Fig. 11n–p), indicating that the level of $LCR^{\Delta F\text{-box}}$ protein also increased (Supplementary Fig. 11q, r). By treating LCR4m with MG132 (a 26S proteasome inhibitor), we also found that the degradation rate of LCR4m decreased (Supplementary Fig. 11s). These results suggest that LCR may be degraded through the 26S proteasome.

miR394 activated the *REV* and *STM* pathways during AM initiation

To explore the pathways affected by miR394/LCR during AM initiation, we analyzed the transcriptomes of *miR394A-OX*, *mir394a-cr*, *mir394b-1*, *pLCR::LCR4m* and WT (Supplementary Data 3). We conducted RNA sequencing of vegetative shoot apex of plants grown under short-day conditions for 30 days. After strict screening with a cutoff of Log2 (fold change >1) and *p* adjusted (FDR) < 0.05, we identified 2224 differentially expressed genes (DEGs) in the *miR394A-OX* lines, 3002 DEGs in the *miR394a-cr* mutants, 2322 DEGs in the *miR394b-1* mutants and 2539 DEGs in the *pLCR::LCR4m* lines (Supplementary Fig. 12a). Gene Ontology (GO) terms related to post-embryo and leaf development were enriched in the *miR394* mutant and *LCR4m-OX* lines, respectively (Supplementary Fig. 12b). We next used the *k*-means clustering algorithm to cluster all expressed genes, which were categorized into nine co-expression modules. Notably, *LCR4m-OX* displayed a more similar profile to the *miR394b-1* mutant than did *miR394a-cr*, characterized by pathways including photosynthesis (Cluster 2) and leaf development (Cluster 8) (Supplementary Fig. 12c).

Previous reports have shown that AM initiation requires cells to continuously express *STM* and that *REV* can directly activate *STM* expression[10]. Subsequently, cytokinin activates *WUS* expression de novo to establish AMs[11]. Thus, we examined *REV*, *STM*, *WUS* and *CLV3* expression in miR394/*LCR* mutants via qRT-PCR. The results revealed that *REV*, *STM* and *CLV3* expression levels were lower in the *mir394a/b* mutants and *LCR4m-OX* plants than in the WT plants (Supplementary Fig. 12d). However, the difference in *WUS* expression was not significant (Supplementary Fig. 12d). To investigate the expression patterns of *REV* and *STM* in vivo, we crossed the marker lines *pSTM::STM-Venus*[50] and *pREV::REV-Venus*[20] with the *p35S::LCR4m* transgenic lines. In young leaf axils (<P_9), the *STM* signals persisted at the boundaries and SAM in the WT (Fig. 3a). The *STM* signals also remained at the *p35S::LCR4m* boundaries and SAM but were much weaker than those of the WT (Fig. 3b). Starting at P_9, the *STM* signals in the older leaf axils of *p35S::LCR4m* weakened and even completely disappeared at P_{13} (Fig. 3b), whereas *STM* was evidently up-regulated in the WT (Fig. 3a). The low expression of *STM* may explain the deficiency of AMs in *LCR4m-OX* plants. We next asked whether *REV* expression is affected in *p35S::LCR4m* plants. In the WT, *REV-Venus* signals were present in AMs (Fig. 3c). However, *REV* was hardly detectable in AMs or on the adaxial side of the leaf primordia in the *p35S::LCR4m* plants (Fig. 3d). To monitor AM initiation quantitatively, we performed live imaging of leaf axils isolated from the shoot apex and grown under short-day conditions for 17 days. We observed small amounts of axillary bud formation in detached axils of *LCR4m-OX* from $P_{8/9}$ and $P_{10/11}$. Then, we performed time-course live imaging with detached $P_{10/11}$ axils to closely trace *STM* and *REV* expression and AM initiation (Supplementary Fig. 13a, c, e, g). After 24 h of cultivation in growth medium, most axils of *LCR4m-OX* plants lost *STM* and *REV* expression, and cell proliferation stopped, whereas the number of *STM*-expressing cells in the axils of WT plants dramatically increased and AMs emerged (Supplementary Fig. 13b, d, f, h). To determine whether the loss of *STM* and *REV* expression in the leaf axil was responsible for the AM initiation defects, we individually introduced inducible *STM-GR* (glucocorticoid receptor) under the *35S* promoter and *REV-GR* under the *REV* promoter into *LCR4m-OX*. We performed dexamethasone (DEX) induction on *pREV::REV-GR-HA p35S::LCR4m* and *p35S::STM-GR p35S::LCR4m* plants and found that the formation of AMs was restored in both plants (Supplementary Fig. 13i–l). These observations confirmed that the inhibition of *LCR* by miR394 is necessary for promoting *STM* and *REV* expression during AM initiation.

LCR is associated with TPL and mediates ubiquitin modification

To gain further insight into the role of LCR in AM initiation, we evaluated the LCR interactome via immunoprecipitation-mass spectrometry (IP-MS) and identified potential substrates (Supplementary Data 4). We used GFP-trap and protein extracts from *p35S::LCR-GFP*, *p35S::LCR4m-GFP* and *p35S::GFP* transgenic plants for immunoprecipitation. In total, seven significant proteins were selected in two biological replicates (Fig. 4a). These included TOPLESS (TPL), SERRATE (SE), HNRNP R-LIKE PROTEIN (HRLP), DOT2, NITRILASE 2 (NIT2), SUPPRESSOR OF MAX2 1 (SMAX1) and AUXIN RESISTANT 6 (AXR6). Among them, TPL was previously characterized as a transcriptional corepressor that interacts with *WUS* to regulate SAM maintenance[21,51]. Notably, TPL and LCR were colocalized in the nuclei of the leaf protoplasts (Supplementary Fig. 14d). We also obtained *p35S::TPL-mCherry* *p35S::*$LCR^{\Delta F\text{-box}}$*-GFP* transgenic plants and observed colocalized signals in the nuclei of the roots (Supplementary Fig. 14a–c, e). We thus tested whether LCR can interact with TPL. As expected, yeast two-hybrid (Y2H) assays revealed that LCR proteins strongly interact with TPL (Fig. 4b). Domain deletion analysis revealed that the C-terminus of LCR (164-467 aa) was required for the interaction (Fig. 4b). Moreover, truncated TPL containing only aa 93 to 352 could interact with LCR (Supplementary Fig. 15a, b). Furthermore, bimolecular fluorescence complementation (BiFC) using *LCR/*$LCR^{\Delta F\text{-box}}$*-cYFP* and *TPL-nYFP* in *Nicotiana benthamiana* epidermal cells confirmed that LCR physically interacted with TPL in nuclei in vivo (Fig. 4c). To confirm the LCR-TPL interaction in *Arabidopsis*, we generated *p35S::LCR4m-GFP* transgenic plants and performed a coimmunoprecipitation (Co-IP) assays. Consistent with the above results, LCR coimmunoprecipitated with endogenous TPL (Supplementary Fig. 14f). *Arabidopsis* expresses five TOPLESS RELATED (TPR) proteins in total, namely, TPL, TPR1 (TOPLESS-RELATED 1), TPR2 (TOPLESS-RELATED 2), TPR3 (TOPLESS-RELATED 3) and TPR4 (TOPLESS-RELATED 4)[21]. Therefore, we tested the potential interaction between LCR and TPL homologs via Y2H and found that LCR may interact with TPR1, TPR2 and TPR4 (Supplementary Fig. 15c, d).

We next investigated whether the expression and/or protein levels of *TPL* were altered by *LCR*. Compared with those in the WT, *TPL* and *TPR1* were slightly down-regulated and *TPR3* was slightly up-regulated in *pLCR::LCR4m*, but the expression of *TPR2* and *TPR4* was not significantly affected by *pLCR::LCR4m* (Supplementary Fig. 16a). To analyze TPL protein levels, we individually transformed *p35S::TPL-mCherry* into WT and *p35S::LCR4m-GFP* plants (Supplementary Fig. 14a–c). Immunoblot analysis revealed obviously reduced TPL-mCherry levels in the LCR4m background (Supplementary Fig. 16b, c).

https://doi.org/10.1038/s41467-024-54494-6

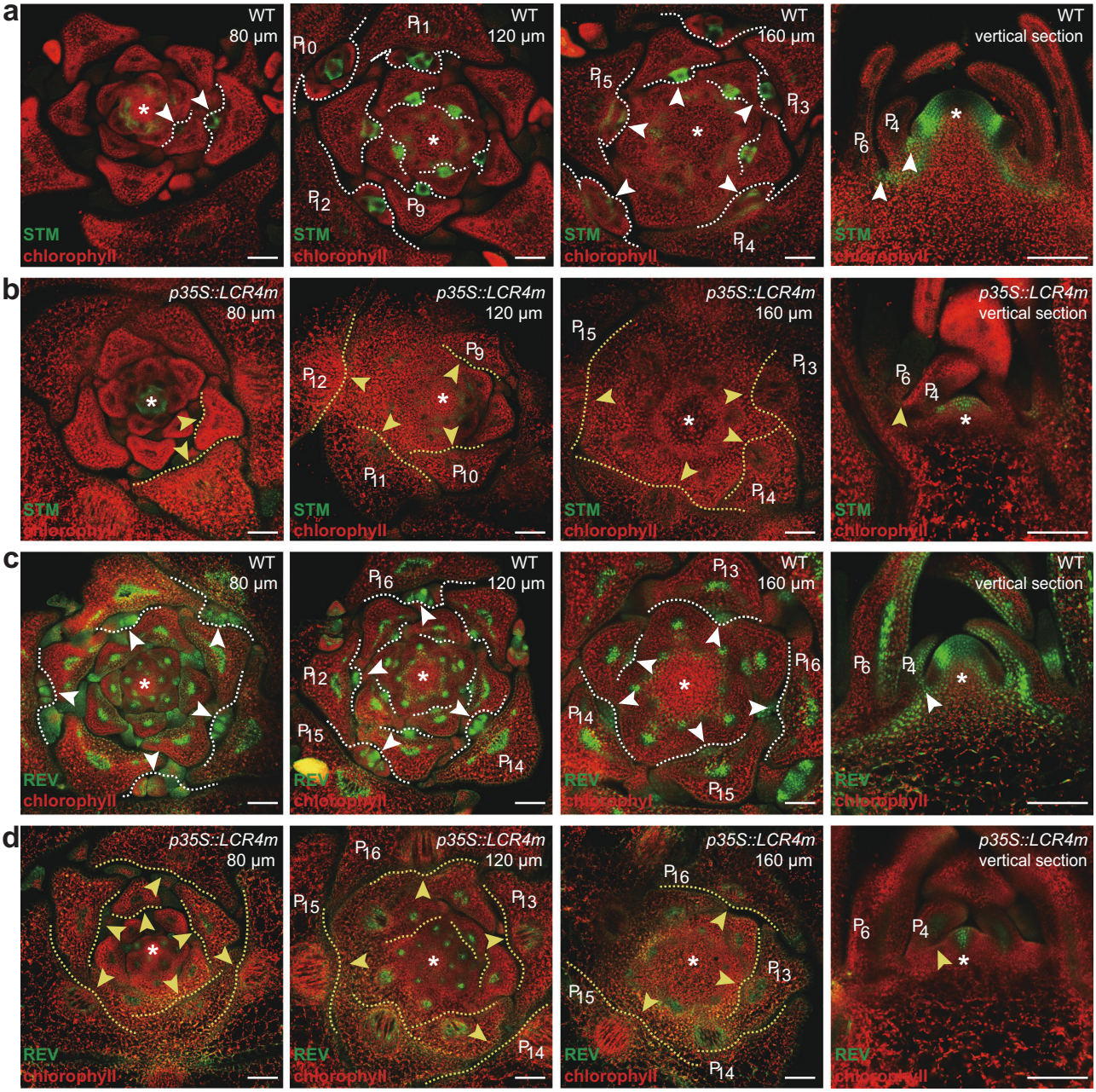

Fig. 3 | REV and STM expression patterns in *LCR4m* transgenic lines. Continuous transverse sections and longitudinal sections showing *pSTM::STM-Venus* (green) expression and chlorophyll autofluorescence (red) in the shoot apex of the WT (**a**) and *p35S::LCR4m* (**b**) plants. STM was activated in AMs of WT plants (white arrows) but maintained low expression levels in the leaf axils of *p35S::LCR4m* plants (yellow arrows). Continuous transverse sections and longitudinal sections of *pREV::REV-Venus* (**c**) and *pREV::REV-Venus p35S::LCR4m* (**d**) shoot apex. REV (green) signals were strong in the AMs (white arrow) of the WT but were extremely weak in the leaf axils of *p35S::LCR4m* (yellow arrows). The asterisks represent the SAM, the arrows represent AMs, and the dashed lines represent the leaf axils where AMs were initiated. The numbers in the upper right corner represent the relative distances from the shoot apex. All the plants were grown under short-day conditions for 30 days. Scale bars, 100 μm. At least three samples were analyzed in (**a**–**d**) with similar results for each experiment.

Moreover, LCR4m-GFP abundance was also significantly lower in *p35S::LCR4m-GFP p35S::TPL-mCherry* transgenic plants than in *p35S::LCR4m-GFP* transgenic plants (Supplementary Fig. 16b, c). To reinforce this conclusion, we also observed the fluorescence signals of *p35S::TPL-mCherry*, *p35S::LCR4m-GFP* and *p35S::LCR4m-GFP p35S::TPL-mCherry* in roots and shoots. Both the LCR and TPL signals were drastically reduced in the roots but absent from the shoots of *p35S::LCR4m-GFP p35S::TPL-mCherry* (Supplementary Fig. 16d).

LCR plays a major role in the Skp1/Cullin1/F-box (SCF) E3 ligase complex[47] and performs its ubiquitination function through the F-box domain (Supplementary Fig. 6). Thus, we hypothesized that LCR may be able to ubiquitinate TPL. To test this hypothesis, we overexpressed *TPL-GFP* in WT and *lcr-1* (Supplementary Fig. 14a–c) and performed immunoprecipitation with an anti-GFP antibody. Subsequent immunoblot analysis of the IP proteins via anti-Ubi antibodies revealed that TPL was ubiquitinated in planta. The level of TPL ubiquitination was lower in *lcr-1* than in WT (Supplementary Fig. 16e). Previous studies revealed that most ubiquitylation of target proteins is associated with 26S proteasome-mediated degradation[25,48]. To confirm whether TPL degradation was mediated by the 26S proteasome, we prepared total

https://doi.org/10.1038/s41467-024-54494-6

a Potential candidate proteins interacting with LCR identified by IP-MS.

Name	Accession	Annotation	Peptides
TPL	AT1G15750	WD40 repeats protein.	5
SE	AT2G27100	C2H2 zinc-finger protein.	23
HRLP	AT2G44710	RNA binding protein.	1
DOT2	AT5G16780	SART-1 family.	3
NIT2	AT3G44300	Nitrilase 2.	4
SMAX1	AT5G57710	Suppressor of max21.	1
AXR6	AT4G02570	Auxin cullin protein.	1

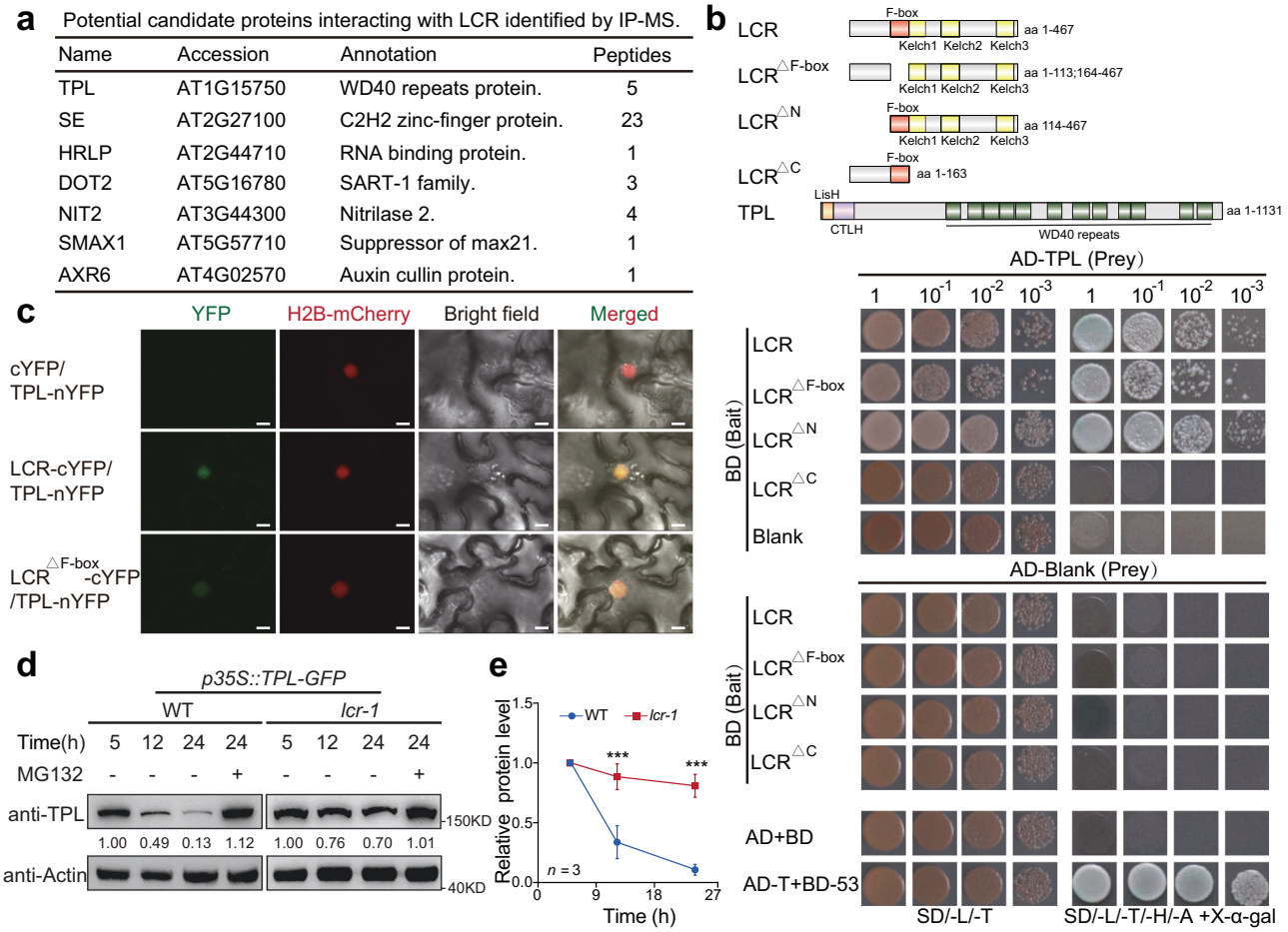

Fig. 4 | LCR associates with TPL. a IP-MS using *p35S::LCR-GFP* and *p35S::LCR4m-GFP* as baits to identify LCR-interacting proteins in *Arabidopsis thaliana*. Important proteins are shown in the list. *p35S::GFP* served as the negative control. **b** The interaction between LCR and TPL was verified via Y2H assays. The protein domains of LCR and TPL used in Y2H are shown at the top. Yeast cells transformed with BD-LCR, BD-LCR$^{F\text{-}box}$ and BD-LCR$^{\Delta N}$/AD-TPL were grown and turned blue on SD-L/-T/-H/-A + X-α-gal medium. Yeast transformed with BD-LCR$^{\Delta C}$/AD-TPL or BD-LCR/AD-Blank did not grow on SD-L/-T/-H/-A + X-α-gal medium. pGADT7-T and pGBKT7-53 were used as positive controls, whereas empty vectors were co-transformed as negative controls. **c** BiFC assays revealed that LCR and LCR$^{\Delta F\text{-}box}$ interacted with TPL in vivo in *N. benthamiana* (tobacco) leaves. H2B-mCherry is a nuclear-localized marker. The combination of *35S::cYFP* and *35S::TPL-nYFP* was used as a negative control. Scale bars, 5 μm. **d**, **e** Stability test of TPL in the WT and *lcr-1* backgrounds. Total protein was extracted from *p35S::TPL-GFP* (blue) and *p35S::TPL-GFP lcr-1* (red) plants with or without MG132 treatment. TPL degradation was measured by immunoblotting with an anti-TPL antibody at the indicated time points. Actin was used as a loading control. Band intensities were quantified with ImageJ in (**e**). Data are mean ± s.d. (***$p < 0.001$, ns no significant difference, two-way ANOVA with Tukey's honestly significant difference test. $n = 3$ biological replicates). The experiments in (**b**–**e**) were performed at least three times with similar results.

protein extracts from *p35S::TPL-GFP* and *p35S::TPL-GFP lcr-1* seedlings at the indicated time points. We found that TPL in protein extracts from *lcr-1* plants degraded more slowly than TPL protein from WT plant extracts did. The addition of the proteasome inhibitor MG132 further decreased the rate of TPL degradation (Fig. 4d, e). These results indicated that the LCR and TPL proteins physically interact with each other and that LCR may negatively regulate TPL abundance via protein degradation.

TPL is expressed in leaf axils and promotes AM initiation

We were curious to know whether TPL regulates AM initiation. For this purpose, we carefully observed the AM phenotype of the *tpl* mutants. The strong allele *tpl-1* with a point mutation (N176H)[21] acts as a dominant negative mutant for multiple TPR family members and displays severe shoot defects and the absence of normal AMs (see below and Supplementary Fig. 18a). Therefore, we obtained another moderate mutant, *tpl* (SALK_097230), with a T-DNA inserted in the WD40 domain of *TPL*. However, unfortunately, *tpl* did not result in any change in AMs (Supplementary Fig. 17a, b). Considering that TPL/TPR family members share conserved structures and redundantly regulate apical fate during embryogenesis[21,23,25], we inferred that TPL/TPR family proteins may also function redundantly in AM initiation. Therefore, we observed AMs in the *tpr1*, *tpr2*, *tpr3*, *tpr4* mutants and the *tpl tpr1 tpr4* triple mutant. Notably, AMs were not affected in the single mutants but were severely compromised in the triple mutant (Fig. 5a and Supplementary Fig. 17a, b). In support of these observations, we carefully analyzed this defect and found that it originated in *tpl tpr1 tpr4* triple mutant leaf axils (Fig. 5b, c). Anatomical analysis revealed that densely stained cells formed morphologically distinguishable bumps in the WT but were lacking in *tpl tpr1 tpr4* (Fig. 5d–g). Moreover, plants that overexpressed *TPL* normally formed one AM per leaf axil (Fig. 6a, b and Supplementary Fig. 17a, b). To monitor *TPL* expression during AM initiation, we constructed *pTPL::GFP* marker lines and observed strong fluorescence signals in the boundary region, AMs and SAM (Fig. 5h and Supplementary Fig. 14a, b). We also analyzed the expression patterns of other TRR proteins via in situ hybridization. As expected, *TPL* mRNA was widely expressed in the shoot apex and young leaf primordia (more extensively than the position of AM initiation) and was particularly strongly expressed in the SAM, AMs and vasculature, which was consistent with *pTPL::GFP* (Fig. 5i and Supplementary Fig. 17c, g). *TPR1*

https://doi.org/10.1038/s41467-024-54494-6

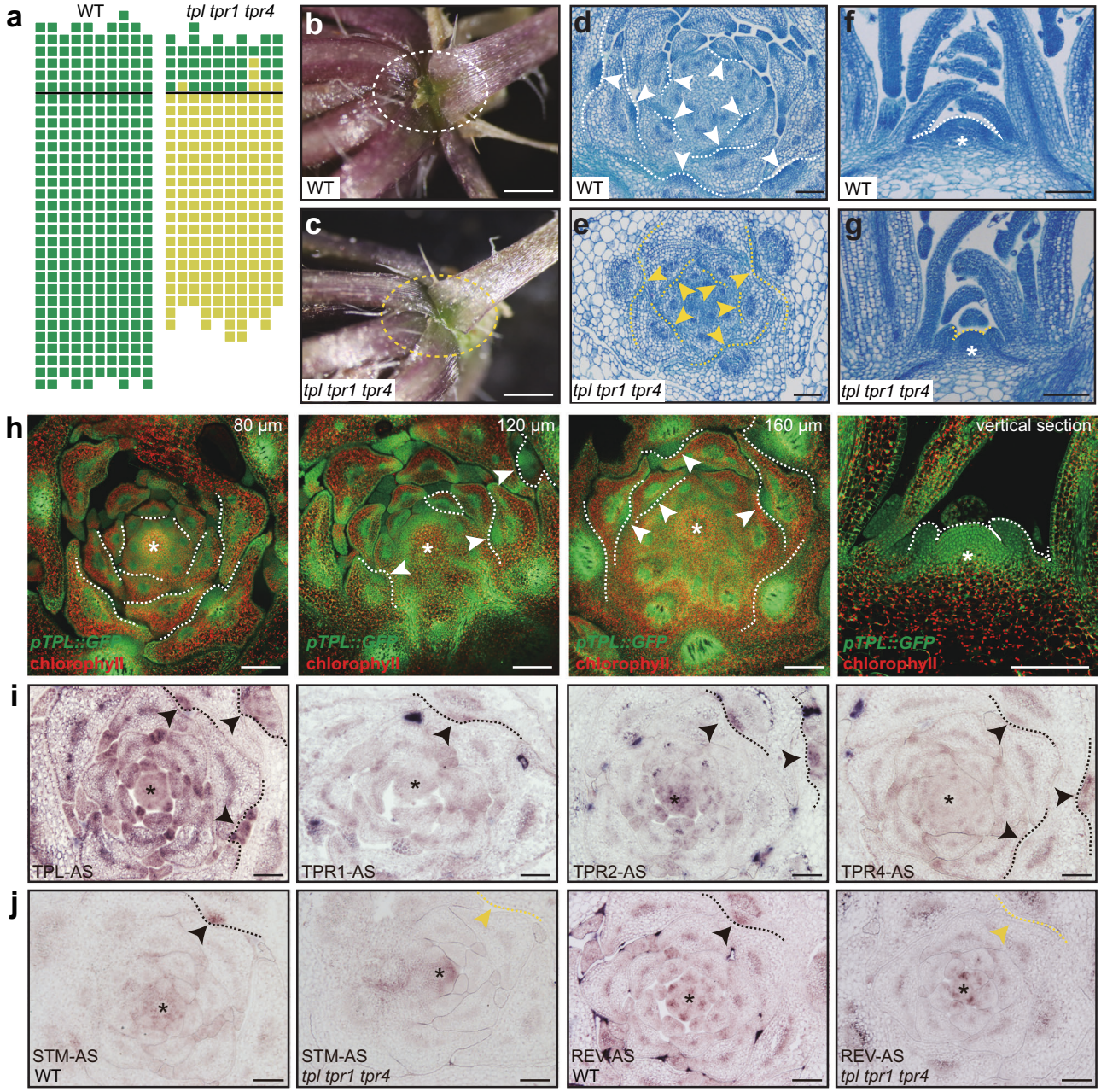

Fig. 5 | *TPL* is expressed in leaf axils and promotes AM initiation. a Schematic representation of AMs in the WT and the *tpl tpr1 tpr4* triple mutant. The diagram is as described in Fig. 1b. Morphology of AMs in the WT (**b**) and the *tpl tpr1 tpr4* triple mutant (**c**). The plants were grown under short-day conditions for 30 days and then transferred to long-day conditions for 30 days. Scale bars, 1 mm. **d**–**g** Cross- and longitudinal sections of shoot apex of WT and the *tpl tpr1 tpr4* triple mutant stained with toluidine blue O. A dome-shaped AM was visible in the WT (arrows, **d**–**f**) but not in the *tpl tpr1 tpr4* triple mutant (yellow arrows, **e**–**g**). All the plants were grown under short-day conditions for 30 days. Scale bars, 100 μm. **h** Expression patterns of *pTPL::GFP* (green) in the vegetative shoot apex. TPL is expressed in leaf axils (dotted white lines), AMs (arrows) and SAMs (asterisks). The numbers in the upper right corner represent the relative distances from the shoot apex. The plants were grown under short-day conditions for 30 days. Scale bars, 100 μm. **i** RNA in situ hybridization was used to determine the expression patterns of *TPL*, *TPR1*, *TPR2* and *TPR4* in the vegetative shoot apex of Col-0. Asterisks indicate SAM, arrows indicate AMs, and dotted lines indicate leaf axils. All the plants were grown under short-day conditions for 30 days. Scale bars, 100 μm. **j** Transverse sections through a vegetative shoot apex showing the distribution of *STM* and *REV* mRNAs in the WT and the *tpl tpr1 tpr4* triple mutant. *STM* accumulated in the SAM and AMs (black arrows) of the WT but not in the AMs of the *tpl tpr1 tpr4* triple mutant (yellow arrows). *REV* was found in the AMs of the WT (black arrows), but no signal was detected in the AMs of the *tpl tpr1 tpr4* triple mutant (yellow arrows). All the plants were grown under short-day conditions for 30 days. Scale bars, 100 μm. At least three samples were analyzed in (**b**–**j**) with similar results for each experiment.

and *TPR4* were detected in the leaf primordia, vasculature, SAM and AMs and largely overlapped with *TPL* (Fig. 5i and Supplementary Fig. 17d, h, f, j). In contrast, *TPR2* was specifically present in the vasculature, boundaries and centers of the SAM and AMs (Fig. 5i and Supplementary Fig. 17e, i). The expression patterns of TPL/TPR family proteins are consistent with their overlapping roles in controlling AM initiation. Moreover, we examined the accumulation of *STM* and *REV* in *tpl tpr1 tpr4* via in situ hybridization. *REV* and *STM* were clearly present in the AMs of WT plants but nearly undetectable in the *tpl tpr1 tpr4* triple mutant (Fig. 5j and Supplementary Fig. 17k–n).

We next analyzed the genetic relationships between *LCR* and *TPL* in AM initiation. For this purpose, we crossed *p35S::LCR4m* with the *tpl-1*

https://doi.org/10.1038/s41467-024-54494-6

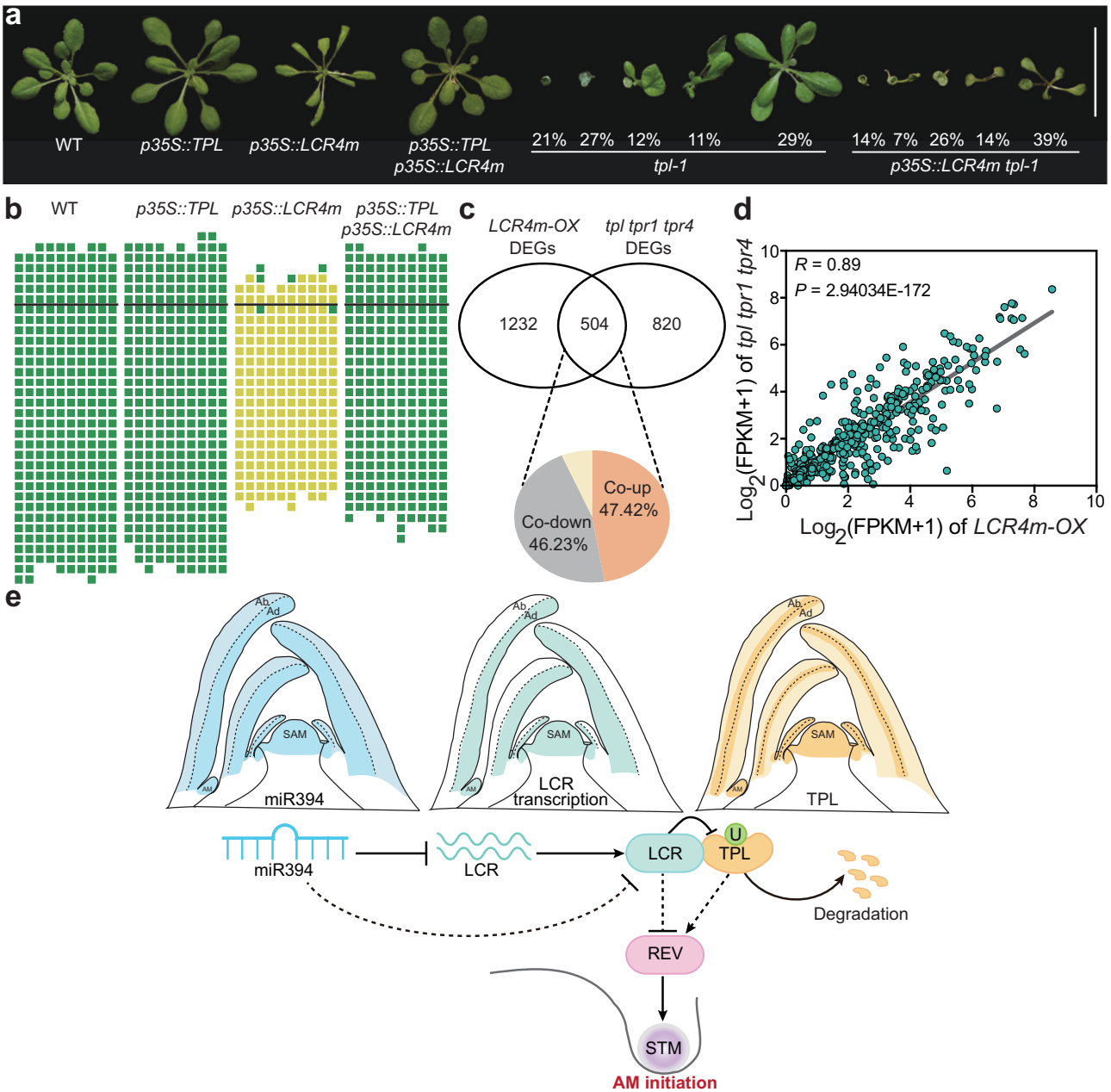

Fig. 6 | *TPL* and *LCR* genetic interactions and a working model for the role of the miR394-LCR-TPL module in regulating AM initiation in *Arabidopsis*. **a** Phenotypes of the WT, *p35S::TPL*, *p35S::LCR4m*, *p35S::TPL p35S::LCR4m*, *tpl-1* and *p35S::LCR4m tpl-1* plants grown for 30 days under short-day conditions. Scale bars, 3 cm. **b** Schematic representation of AMs in the WT, *p35S::TPL*, *p35S::LCR4m* and *p35S::TPL p35S::LCR4m* hybrid generations. The diagram is as described in Fig. 1b. **c** Venn diagram showing the number of overlapping DEGs between the *LCR4m-OX* and *tpl tpr1 tpr4* mutants compared with the WT. The numbers of up-regulated (orange) and down-regulated (gray) DEGs are shown. The vegetative shoot of two biological replicates ($n = 2$) were collected at 30 days under short-day conditions for RNA sequencing. **d** Pearson correlation of common DEGs in *LCR4m-OX* and *tpl tpr1 tpr4*. The numerical values represent the log2 (FPKM+1) in the two samples. *p* values were determined via two-tailed Pearson correlation coefficient analysis. **e** A working model elucidating the crosstalk among miR394, LCR and TPL in AMs. miR394 is expressed in shoot apex and strictly inhibits *LCR* accumulation in leaf axils, to attenuate LCR mediated TPL degradation and activate *REV* and *STM* pathway, which is essential for AM initiation. Ab abaxial axis, Ad adaxial axis. The experiments in (**a**–**d**) were performed at least two times with similar results.

mutant and obtained *p35S::LCR4m tpl-1* plants (Supplementary Fig. 14c). The subsequent phenotyping revealed that the morphology of the *p35S::LCR4m tpl-1* plants was similar to that of the *tpl-1* plants, and the embryos failed to form apical meristems and showed varying degrees of cotyledon fusion (Fig. 6a and Supplementary Fig. 18a). In addition, we discovered that the overexpression of *TPL* rescued the AM deficiency of *p35S::LCR4m*, as reflected by the normal expression of *REV* and *STM* (Fig. 6a, b and Supplementary Fig. 18b). In support of these observations, we compared the transcriptomes of *p35S::LCR4m* and *tpl tpr1 tpr4* in the vegetative shoot apex (Supplementary Data 5). Compared with those in the WT, we identified 1736 DEGs in *p35S::LCR4m* and 1324 DEGs in the *tpl tpr1 tpr4* mutants (FDR < 0.05 and Log2 (fold change) >1). Ultimately, we identified 504 common genes with high confidence, comprising 239 (47.42%) up-regulated genes and 233 (46.23%) down-regulated genes (Fig. 6c). To better understand the relationships among the DEGs associated with *p35S::LCR4m* and *tpl tpr1 tpr4*, we analyzed the 504 DEGs via Pearson correlation analysis. Consistently, these common DEGs were highly correlated ($R = 0.89$) with respect to expression

(Fig. 6d). These results indicated that *LCR* and *TPL* have similar effects on a common set of genes. Collectively, these results demonstrated that *TPL* may act downstream of *LCR* and as a target of LCR to positively regulate AM initiation via the *REV-STM* pathway (Fig. 6e).

Discussion

miRNAs play a vital role in plant development via the precise control of cell proliferation and differentiation[26,27,31]. However, almost no miRNAs have been characterized in AMs until now because of their subtle structure. AMs contain reactivated stem cells and various cell types, which make them representative of tissue development[1–3]. We resorted to a tissue-specific miRNA library and identified key regulators of AM initiation (Fig. 1). The number of cells expressing miR394 is limited in plants because miR394 expression has rarely been detected in libraries of small RNAs generated from whole seedlings. High levels of miR394 are expressed in boundary enrichment tissues, indicating a role of miR394 in the axillary meristem in addition to SAM. There are two copies of miR394 in *Arabidopsis*, of which miR394b plays a dominant role in SAM. Specifically, miR394b is transcribed in the L1 layer of the SAM and moves to the lower layers to execute a non-cell-autonomous role in stem cell maintenance by affecting *WUS-CLV3*[39]. In AMs, miR394a and miR394b collaborate and play overlapping roles in promoting AM initiation, although the miR394b mutant displayed a more severe phenotype of AM deficiency (Fig. 1). *MIR394A* was strongly expressed in L3 and the underlying cells, whereas *MIR394B* was more highly expressed in L1-L3 of the AMs (Fig. 2). In situ hybridization revealed that mature miR394 was distributed in a gradient in AMs, with high expression levels in L1 and lower expression levels underneath (Fig. 2). In contrast, LCR showed the opposite expression pattern from L1 to L3 and in the cells underneath (Fig. 2). *STM* and *REV* expression in AMs indicated that miR394 levels persisted in leaf boundaries to maintain stem cells in younger leaf axils and increased to activate AM initiation in older leaf axils (Fig. 3). *WUS* did not show significant change in shoot apex of *mir394* mutants may be due to tissue dilution. These results demonstrate that miR394 plays a conserved role in stem cell maintenance in both AMs and SAMs and promote meristem initiation in axils.

miRNAs cleave target mRNAs at the posttranscriptional level[30,32,33]. LCR is a reported target of miR394 and encodes an F-box protein[36,44]. Previous studies have shown the role of LCR in SAM and leaf development[39,42,43,45]. Here, genetic and cellular experiments revealed that LCR is expressed in AMs and negatively regulates AM initiation (Figs. 1–3). Furthermore, transgenic lines with truncated LCR indicated that the F-box domain is necessary for LCR function in AMs (Figs. 1 and 2). F-box proteins are well known to be tightly linked to protein ubiquitylation and degradation[52]; however, the substrates of the LCR protein are less well known. Here, we used IP-MS to screen LCR downstream substrates and identified TPL (Fig. 4). TPL was reported to control gene transcription with transcription factors as general repressors[23,24,53]. However, the role of TPL in AMs has not been studied. The phenotyping of *tpl* and homologous mutants revealed significant AM deficiency, similar to the LCR OX lines, indicating that this gene participated in AM initiation and coregulated common genes with LCR (Figs. 5 and 6). The expression of TPL in leaf axils and AMs verified that *TPL* directly regulates AM initiation in leaf axils (Fig. 5). Genetic data confirmed that *LCR* and *TPL* function downstream of miR394 (Fig. 6). Together, these results collectively reveal a pathway comprising miRNAs and F-box-mediated proteins that regulate AM formation.

Previous studies have focused on the transcriptional control of AMs, but the regulation of AMs at the protein level is less well understood[7,8,10,12–14]. AM initiation is a complicated process through which plants build architecture to reach the highest yield and respond to environmental conditions[19]. Here, we studied AM regulation at the protein level. LCR itself was strictly regulated in the shoot apex, as LCR signals were not easily detected in LCR OX and marker lines constructed with the native proteins. Only in mutated versions in which the miR394 binding sites were deleted or the F-box domain was deleted could LCR be detected in the transgenic lines. Nevertheless, the relationship between miR394 cleavage and F-box regulation, i.e., posttranscriptional and translational control of LCR, is not known. LCR, as an F-box protein, interacts with several important substrates related to certain pathways. TPL is a general transcription factor, and SE is a component of dicing bodies, which process small RNAs[22,30]. The interaction of LCR with other proteins, such as SE, deserves further study. In this study, we demonstrated that LCR interacted with TPL and accelerated TPL degradation, likely through ubiquitylation. The modification sites of the TPL and LCR proteins are also not clear. In addition to TPL, its functionally redundant homologs, TPR1, TPR2 and TPR4, also interact with LCR. Thus, LCR may also mediate the ubiquitylation and degradation of other TPR proteins; however, this possibility remains to be further validated. It has been reported that the regulation of *PLETHORA1/2* (*PLT1/PLT2*) expression by *TPL* and *HD-ZIPIII* is necessary for apical/shoot fate in early embryogenesis[54]. In our study, we revealed that *TPL* and *REV* are also necessary for AM initiation confirming the positive roles of *TPL* and *HD-ZIPIII* in meristem development. Interestingly, the expression of *REV* was not observed in the leaf axils of the *tpl tpr1 tpr4* triple mutant indicating that *REV* function downstream *TPL* and *LCR* in AM initiation. In brief, we provide a mechanistic framework to explain how plants regulate AM initiation at the transcriptional, posttranscriptional and protein levels. This framework not only includes a number of newly identified AM-defective mutants but also integrates the known genes *STM* and *REV* in the AM initiation pathway.

Methods

Growth conditions

Arabidopsis thaliana plants were grown at 22 °C under full-spectrum white fluorescent light under short-day (8 h light/16 h dark) or long-day (16 h light/8 h dark) conditions. For molecular identification and sRNA-seq in the seedlings, seeds were geminated on half-strength Murashige and Skoog (1/2 MS) medium and grown under short-day conditions for 10 days (2–4 leaves). For live imaging of the leaf axil regions, plants were grown under short-day conditions for 17 days (about 10–12 leaves). For scanning electron microscopy analysis of P_{15} axillary buds, plants were grown under short-day conditions for 21 days (14–16 leaves). For RNA-seq, sRNA-seq and quantitative analysis of mRNAs in the shoot apex, plants were grown under short-day conditions for 30 days (26–30 leaves). For sectioning and gene expression pattern analysis in the shoot apex, plants were grown under short-day conditions for 30 days before paraffin or low-melting point agarose sectioning. For AM phenotyping, plants were grown under short-day conditions for 30 days and then under long-day conditions for an additional 30 days to induce flowering before the axillary buds were counted.

Genetic material

Arabidopsis thaliana ecotypes Columbia (Col-0) and Landsberg *erecta*−0 (L*er*) were used as wild-type controls. The *mir394b-1* (single nucleotide mutation, G110A)[39], *tpl* (SALK_097230)[55], *tpr1* (mos10)[55], *tpr2* (SALK_112730)[56], *tpr3* (WiscDsLox350C06)[56], *tpr4* (SALK_150008)[55] and *tpl tpr1 tpr4*[55] mutants are in the Col-0 background. The *tpl-1* (point mutation, N174H)[21] mutants are in the L*er* background. The transgenic lines *pTPL::TPL*[53] and *pREV::REV-GR-HA*[57] are in the Col-0 background. The *pREV::REV-Venus*[20], *pSTM::STM-Venus*[20] and *p35S::STM-GR*[58] lines are in the L*er* background. The *mir394b-1* was kindly provided by Xuemei Chen (Peking University). The *tpl-1* and *pTPL::TPL* were kindly provided by Lei Wang (Institute of Botany, CAS). The *tpl*, *tpr1*, *tpr2*, *tpr3*, *tpr4* and *tpl tpr1 tpr4* were kindly provided by Jingbo Jin (Institute of Botany, CAS).

In this study, *lcr-1* (SALK_136833) mutants were obtained from the AraShare *Arabidopsis* Stock Center. The *mir394a-cr*, *mir394b-cr* and *lcr-cr* mutants were generated via a CRISPR-Cas9 system in the Col-0 background. The *mir394a/b* double mutant was obtained via genetic crosses of *mir394a-cr* and *mir394b-1*. The *mir394a/b lcr-1* triple mutant was generated via a genetic cross of *mir394a/b* and *lcr-1*. The *pREV::REV-Venus p35S::LCR4m*, *pSTM::STM-Venus p35S::LCR4m*, *pREV::REV-GR-HA p35S::LCR4m*, *p35S::STM-GR p35S::LCR4m and p35S::LCR4m tpl-1* were generated via genetic crosses. The *p35S::MIR394A*, *p35S::MIR394B*, *p35S::LCR*, *p35S::LCR4m*, *p35S::LCR5m*, *p35S::LCR$^{F\text{-}box}$*, *p35S::LCR4m$^{\Delta F\text{-}box}$*, *pLCR::LCR*, *pLCR::LCR4m*, *pLCR::LCR$^{\Delta F\text{-}box}$*, *pLCR::LCR4m$^{\Delta F\text{-}box}$*, *pMIR394-A::GFPer*, *pMIR394B::GFPer*, *gLCR::GFP*, *pREV::LCR5m*, *pKAN1::LCR5m* and *pTPL::GFP* transgenic lines were generated in the Col-0 background. The *p35S::TPL-GFP* transgenic lines were individually generated in the Col-0 and *lcr-1* backgrounds. The *p35S::TPL-mCherry* transgenic lines were individually generated in the Col-0, *p35S::LCR$^{\Delta F\text{-}box}$* and *p35S::LCR4m* backgrounds. All the transgenic lines used in this work were generated via the *Agrobacterium*-mediated GV3101 transformation method. For selection of transgenic plants, seeds were sterilized and germinated on MS medium supplemented with 25 mg/L hygromycin or 50 mg/L kanamycin. The mentioned material genotyping primers are listed in Supplementary Table 1.

Vector construction

To construct the *mir394a-cr*, *mir394b-cr* and *lcr-cr* mutants, the sgRNA sequence targeting *pre-miR394a*, *pre-miR394b* or *LCR* was synthesized and inserted into the *pBUE401* CRISPR/Cas9 vector using the BsaI enzyme (NEB)[59]. To construct the expression vector, *MIR394A* (3000 bp promoter) and *MIR394B* (3000 bp promoter) were amplified from Col-0 genomic DNA and inserted into the *TSK108* vector, and subsequently, constructed into the *pMDC204* vector via gateway. The genomics-*LCR* (2281 bp promoter and the first exon, intron, and three amino acids of the second exon) and promoter-*TPL* (2548 bp promoter) were amplified from Col-0 genomic DNA and inserted into the *pCambia1300* vector via homologous recombination constructs. To construct the *LCR* overexpression vector, the *LCR* (the first exon, intron, and the second exon) was amplified from Col-0 genomic DNA. The *LCR4m* and *LCR5m* were constructed by point mutations[39,43]. The *LCR$^{\Delta F\text{-}box}$* and *LCR4m$^{\Delta F\text{-}box}$* were amplified from two fragments via the corresponding primers to remove the F-box region. The PCR fragments were subsequently cloned and inserted into the *pGEM-T Easy vector* (Promega) and individually transferred into the *LCR* promoter and *35S* promoter-driven expression vector *pCambia1300* via digestion and ligation. To construct the LCR ectopic expression vector, *REV* (3000 bp promoter) and *KAN1* (3000 bp promoter) were amplified from Col-0 genomic DNA and inserted upstream of the *LCR5m* coding sequence (CDS). The fragment was subsequently introduced into the express vector *pCambia1300*. To construct the *TPL* overexpression vector, the CDS of *TPL* was amplified from Col-0 cDNA and individually introduced into the expression vectors *pCambia2300* and *pCambia1300* driven by the *35S* promoter. The primers used for vector construction are listed in Supplementary Table 1.

Total RNA extraction, qRT-PCR analysis and northern blotting

Total RNA was extracted from 30-day-old vegetative shoot apices via TRIzol reagent (Invitrogen, Carlsbad, CA, USA) and treated with RNase-free DNase I (Thermo Fisher). First-strand cDNA was synthesized with 1 ng of total RNA via oligo-dT primers and the HiScript III 1st Strand cDNA Synthesis Kit (Vazyme, Nanjing, China) according to the manufacturer's instructions. qRT-PCR was performed using Hieff qPCR SYBR Green Master Mix (Yeasen, Shanghai, China) according to the manufacturer's instructions on a Bio-Rad CFX96 real-time PCR detection system with a KAPA SYBR FAST qPCR kit (KAPA Biosystems, Beijing, China). *ACTIN2* was used to normalize the relative expression. The qRT-PCR primers (Supplementary Table 1) were used to amplify each gene. The mRNA expression levels were calculated via the $2^{-\Delta\Delta Ct}$ method. The data were repeated with three biological and at least two technical replicates.

For small RNA northern blotting[60]. Total RNA (10 μg) was resolved on 15% urea-PAGE gels and then transferred to a nylon membrane for 1 h at 300 mA. The nylon membrane was subsequently hybridized overnight at 50 °C with 3' biotin-marked DNA probes to detect miRNAs. The probes used are listed in Supplementary Table 1.

RNA-seq and sRNA-seq

For RNA-seq, vegetative shoot apex materials (grown under short-day conditions for 30 days) were collected from *mir394b-1*, *mir394a-cr*, *pLCR::LCR4m*, *miR394A-OX*, *p35S::LCR4m*, *tpl tpr1 tpr4* and WT individually for RNA extraction. An RNA-seq libraries were constructed via standard Illumina protocols. Deep sequencing was performed via an Illumina NovaSeq 6000 platform in 150-nucleotide paired-end mode by Berry Genomics (Beijing). Two biological replicates were prepared and analyzed for each sample. Each replicate was obtained by pooling samples from at least fifty plants. The raw sequencing reads were quality trimmed via Trim Galore (v0.6.5), and the clean reads were mapped to the *Arabidopsis thaliana* reference genome sequence (TAIR10 Genome Release) via HISTA2 (v2.2.1)[61]. The count files were then used as input for DEG analysis via DESeq2 (v1.36.0)[62] with the threshold of Log2 (fold change) >1 and an FDR < 0.05 were set as the cut off criteria for significant differences. The raw counts were further normalized to fragments per kilobase of transcript per million fragments mapped (FPKM). Gene co-expression models of all DEGs were constructed using the *k*-means method by *Z*-scaled FPKM in R (v4.0.2), and the cluster number was determined by the figure of merit approach[63]. The gene expression heat map was displayed using the R package ComplexHeatmap (v2.4.3)[64]. Functional enrichment was performed via the R package clusterProfiler (v4.0)[65], and GO annotation files were generated from TAIR Annotation. Correlation coefficients represent the distance between any two samples, and data were conducted by Cor function in R (v4.0.2)[66].

For sRNA-seq, the seedlings of Col-0 grown under short-day conditions for 10 days and vegetative shoot apex of Col-0 grown under short-day conditions for 30 days were collected with two biological replicates, individually. The sRNA-seq libraries were prepared from 1 μg of total RNA via standard Illumina protocols. Deep sequencing was performed with insertions between 18 and 40 bp on an Illumina NextSeq 500 by Berry Genomics (Beijing). The raw sRNA-seq data were trimmed via Cutadapt (v1.12)[67] to remove adapters and low-quality reads. Reads that were 18–30 nt in length were retained. The retained reads were annotated via the Infernal package (v1.1.2) in Rfam (https://www.sanger.ac.uk/tool/rfam/). The number of reads mapped to known miRNA sequences was determined via FeatureCounts (v2.0.0)[68] on the basis of the *Arabidopsis* miRNA models in miRBase (release 22.1). The transcription levels of the miRNAs were estimated via the R package edgeR[69] on the basis of the read counts, which were normalized to CPM (read counts per million mapped reads) values. DE miRNAs were identified via DEseq2 (v1.36.0)[62] with the threshold of Log2 (fold change) >1 and an FDR < 0.05.

Observation of the AM phenotype

For visualization of AMs, plants were placed under a stereoscope, and observed whether buds had formed in the leaf axils of rosette and cauline leaves in order from the oldest to the youngest leaf axils. Among them, the cotyledons did not form AM, so the cotyledons were removed during the statistical analysis. We performed at least three independent biological experiments, and more than 20 individual plants were counted each time.

Live imaging

For live imaging[10,70], leaves between P_8 and P_{11} were detached from seedlings using dissecting medium (3% agarose) and laid flat on

imaging medium (1/2 MS medium with 1% agarose on the top). FM4-64 (Thermo Fisher) was applied to the meristem for 20 min for imaging. For time-lapse live imaging, the leaves were transferred back to growth medium (1/2 MS medium with 2% sucrose, 0.0005% (w/w) folic acid, 0.01% (w/w) myo-inositol, pH 6.0 and 0.3% phytagel) under normal growth conditions after each image. All live imaging experiments were performed via the water dipping lens of an Olympus (FV1000MPE) confocal microscope.

Agarose sectioning

For agarose sectioning, shoot apex were collected by removing the leaves and then immediately placed in 2.5% paraformaldehyde (PFA; Sigma-Aldrich) at pH 7.0. After vacuum infiltration for 30 min on ice, the samples were stored overnight at 4 °C. Fixed tissue samples were washed with 10% sucrose (prepared with 1% PFA at pH 7.0) for 20 min, 20% sucrose (prepared with 1% PFA at pH 7.0) for 20 min, and 30% sucrose (prepared with 1% PFA at pH 7.0) for 30 min, successively. The samples were then embedded in 6% low-melting-point agarose (Promega) liquid gel at 37 °C and placed at 4 °C for 30 min to solidify. Sections (40 μm) were prepared using a Leica VT1000S vibratome.

TBO staining and RNA in situ hybridization

For TBO staining[71] and RNA in situ hybridization[72,73], the shoot apex were harvested and fixed with 4% paraformaldehyde. After being embedded in wax, the sections were sliced into 8 μm sections using a Leica instrument (RM2255). The miR394 probes were synthesized via LNA modification, and 3′ digoxigenin-labeled mRNA probes were amplified from Col-0 cDNA with gene-specific primers containing the T7 promoter sequence at the 5′ end and synthesized using a DIG Northern Starter Kit (Roche, 11277073910). The primers used for probe synthesis are detailed in Supplementary Table 1.

Subcellular localization

For colocalization of LCR and TPL in *Arabidopsis* protoplasts, the CDS of *LCR* was amplified and ligated into *pBI221-GFP*, and *TPL* was amplified and ligated into the *pBI221-mCherry* vector. All primers used are listed in Supplementary Table 1. The plasmids were subsequently transformed into protoplasts obtained from the leaf sheaths of 21-day-old seedlings via the polyethylene glycol-mediated transient expression system. The transformed protoplasts were observed via confocal microscopy.

BiFC assays

The full-length CDS of the *TPL* sequence was recombined into *pSPYNE*, while the CDS of *the LCR* and $LCR^{\Delta F\text{-}box}$ sequences were recombined into *pSPYCE*. All primers used for BiFC are listed in Supplementary Table 1. Each construct was subsequently introduced into *Agrobacterium* GV3101. Then, different combinations were co-infiltrated into 4-week-old *N. benthamiana* leaves as indicated for transient expression. H2B-mCherry was used as a nuclear marker. After co-transformation for 36–48 h, the YFP signals were analyzed via confocal microscopy.

Confocal microscopy, optical microscopy, and scanning electron microscopy

Confocal microscopy images were taken with a Zeiss (LSM 980) or an Olympus (FV1000 MPE) microscope. The excitation and detection wavelengths were 488 nm and 505–525 nm for GFP; 488 nm and 650–700 nm for autofluorescence; 514 nm and 580–620 nm for FM4-64, 514 nm and 524–550 nm for Venus; and 561 nm and 585–640 nm for mCherry. Optical photographs were taken with an Olympus (BX53) microscope equipped with a Canon camera. Scanning electron microscopy was performed by using a Hitachi S-4800 field-emission variable pressure scanning electron microscope after standard tissue preparation for cellular observation. We observed at least three independent transgenic lines in each genetic background and confirmed that the patterns were consistent within each genotype.

Chemical treatments

For Dex treatment, a 10 μM Dex (Sigma-Aldrich) solution containing 0.01% (v/v) Silwet-77 was applied to vegetative shoot apex tissues every two days. After 30 days of continuous treatment, the plants were transferred to long-day conditions for 30 days, and the AM initiation phenotype was observed.

For MG132 treatment, equal numbers of seedlings were cut into 1–2 mm slices and treated with 50 μM MG132 (Sigma-Aldrich) solution or without MG132 (0.1% DMSO) for 5 h (exposed to light) or 24 h (exposed to the dark). Samples were collected at 5, 12 and 24 h after treatment for protein extraction and detected by immunoblotting.

Protein extraction and immunoprecipitation

For total protein extraction, seedlings were harvested and ground in liquid nitrogen, and the powder was resuspended in IP buffer (50 mM Tris-HCl (pH 7.5), 0.5 mM EDTA (pH 8.0), 150 mM NaCl, 2 mM $MgCl_2$, 1 mM DTT, 0.5% NP-40, 1 mM PMSF, 2 mM NaF, 50 μM MG132 and 1x proteinase inhibitor cocktail (Roche)) and incubated for 30 min with gentle rotation at 4 °C. The protein suspensions were centrifuged at 15,000 × *g* for 10 min (repeated once) to remove debris, and the supernatant was collected for further experiments.

For IP-MS, the same protein extraction procedure was individually performed for 2 g of *p35S::LCR-GFP*, *p35S::LCR4m-GFP* and *p35S::GFP* seedling material. The supernatant was supplemented with precleared GFP Trap beads (ChromoTek) and incubated at 4 °C with gentle agitation for 2 h. The beads were washed at least five times with washing buffer-1 (50 mM Tris-HCl (pH 7.5), 0.5 mM EDTA (pH 8.0), 150 mM NaCl, 0.5% NP-40, 1 mM DTT, 1 mM PMSF and 50 μM MG132) and washing buffer-2 (50 mM Tris-HCl (pH 7.5), 0.5 mM EDTA (pH 8.0), 150 mM NaCl, 1 mM PMSF and 50 μM MG132). Finally, the protein-bead complex was separated via sodium dodecyl sulfate-polyacrylamide gel electrophoresis (SDS-PAGE). After Coomassie blue staining, the target gel lanes were cut and sliced, and digestion was carried out with trypsin. After staining and trypsin digestion, the polypeptide was subjected to mass spectrometry via an Orbitrap Fusion Lumos instrument (Thermo Fisher Scientific) from the CAS Centre of the Institute of Botany, Key Laboratory of Plant Molecular Physiology. The search engine was used for protein identification by searching against the UniProt protein database (https://www.uniprot.org/). The false discovery rate (FDR) for protein identification was also set at 0.01. The significance threshold was set at $p < 0.05$.

For Co-IP, the WT, *tpl tpr1 tpr4* and *p35S::LCR4m-GFP* supernatants were incubated with GFP-Trap for 2 h at 4 °C, after which the beads were washed with washing buffer-1 and washing buffer-2 three times. The protein was eluted from the beads in 2XSDS sample buffer (120 mM Tris-HCl (pH 6.8), 20% glycerol, 4% SDS, 0.04% bromophenol blue, and 10% β-mercaptoethanol) by heating at 95 °C for 5 min. The proteins were subsequently transferred to 8% SDS-PAGE gels and detected with anti-GFP and anti-TPL antibodies.

For in vivo ubiquitination assays, the *p35S::TPL-GFP* and *p35S::TPL-GFP lcr-1* protein supernatants were incubated with GFP-Traps for 2 h at 4 °C and detected with anti-GFP and anti-ubiquitin antibodies.

The primary antibodies used in this study included anti-GFP (598, MBL, 1:1000 dilution), anti-mCherry (PM005, MBL, 1:1000 dilution), anti-ubiquitin (Ab134953, Abcam, 1:1000 dilution), anti-TPL (A21285, ABclonal, 1:1000 dilution) and anti-ACTIN (AC009, ABclonal, 1:3000 dilution) antibodies. The expression of protein was counted using ImageJ (National Institutes of Health, USA) per sample.

Y2H assays

LCR, *TPL*, *TPR1*, *TPR2*, *TPR3* and *TPR4* were amplified from Col-0 cDNA and subsequently cloned and inserted into the prey vector *pGADT7*

(630442, Clontech) or bait vector *pGBKT7* (630443, Clontech). The primers are listed in Supplementary Table 1. Standard yeast extract-peptone-dextrose plus adenine (YPAD) media were used, and a lithium acetate protocol was used to transform the digested plasmids. The yeast strain AH109 was co-transformed with various bait and prey construct combinations via heat shock treatment (42 °C, 15 min). Equal numbers of co-transformed yeast cells were grown on SD-Leu/-Trp medium for 3 days (30 °C). The relevant yeast cells were serially diluted (1:10, 1:100, 1:1000) and added to SD-Leu/-Trp/-His/-Ade solid selective medium containing X-α-gal to detect protein interactions.

Statistics and reproducibility

Statistical analyses to examine significant differences and result visualization were performed with the GraphPad Prism 9 software. Significance was determined by $p < 0.05$ [*] or $p < 0.01$ [**]. All gel blots/plots were performed at least three times.

Reporting summary

Further information on research design is available in the Nature Portfolio Reporting Summary linked to this article.

Data availability

The raw data of regular RNA-Seq and small RNA-Seq in this study have been deposited in National Centre for Biotechnology Information (NCBI) (accession numbers PRJNA1101744 and PRJNA1164152). All plasmids and strains supporting the finding of this study are available from the corresponding author upon request. Source data are provided with this paper.

References

1. Burian, A., Barbier de Reuille, P. & Kuhlemeier, C. Patterns of stem cell divisions contribute to plant longevity. *Curr. Biol.* **26**, 1385–1394 (2016).
2. Dinneny, J. R. & Benfey, P. N. Plant stem cell niches: standing the test of time. *Cell* **132**, 553–557 (2008).
3. Kaufmann, K., Pajoro, A. & Angenent, G. C. Regulation of transcription in plants: mechanisms controlling developmental switches. *Nat. Rev. Genet.* **11**, 830–842 (2010).
4. Schmitz, G. & Theres, K. Shoot and inflorescence branching. *Curr. Opin. Plant Biol.* **8**, 506–511 (2005).
5. Grbić, V. & Bleecker, A. B. Axillary meristem development in *Arabidopsis thaliana*. *Plant J.* **21**, 215–223 (2000).
6. Long, J. & Barton, M. K. Initiation of axillary and floral meristems in *Arabidopsis*. *Dev. Biol.* **218**, 341–353 (2000).
7. Chahtane, H. et al. A variant of *LEAFY* reveals its capacity to stimulate meristem development by inducing *RAX1*. *Plant J.* **74**, 678–689 (2013).
8. Greb, T. et al. Molecular analysis of the *LATERAL SUPPRESSOR* gene in *Arabidopsis* reveals a conserved control mechanism for axillary meristem formation. *Genes Dev.* **17**, 1175–1187 (2003).
9. Raman, S. et al. Interplay of miR164, *CUP-SHAPED COTYLEDON* genes and *LATERAL SUPPRESSOR* controls axillary meristem formation in *Arabidopsis thaliana*. *Plant J.* **55**, 65–76 (2008).
10. Shi, B. et al. Two-step regulation of a meristematic cell population acting in shoot branching in *Arabidopsis*. *PLoS Genet.* **12**, e1006168 (2016).
11. Wang, J. et al. Cytokinin signaling activates *WUSCHEL* expression during axillary meristem initiation. *Plant Cell* **29**, 1373–1387 (2017).
12. Xin, W., Wang, Z., Liang, Y., Wang, Y. & Hu, Y. Dynamic expression reveals a two-step patterning of *WUS* and *CLV3* during axillary shoot meristem formation in *Arabidopsis*. *J. Plant Physiol.* **214**, 1–6 (2017).
13. Yang, F., Wang, Q., Schmitz, G., Müller, D. & Theres, K. The bHLH protein ROX acts in concert with *RAX1* and *LAS* to modulate axillary meristem formation in *Arabidopsis*. *Plant J.* **71**, 61–70 (2012).
14. Zhang, C. et al. Spatiotemporal control of axillary meristem formation by interacting transcriptional regulators. *Development* **145**, dev158352 (2018).
15. Talbert, P. B., Adler, H. T., Parks, D. W. & Comai, L. The *REVOLUTA* gene is necessary for apical meristem development and for limiting cell divisions in the leaves and stems of *Arabidopsis thaliana*. *Development* **121**, 2723–2735 (1995).
16. Otsuga, D., DeGuzman, B., Prigge, M. J., Drews, G. N. & Clark, S. E. *REVOLUTA* regulates meristem initiation at lateral positions. *Plant J.* **25**, 223–236 (2001).
17. Zhang, C. et al. Regulation of *ARGONAUTE10* expression enables temporal and spatial precision in axillary meristem initiation in *Arabidopsis*. *Dev. Cell* **55**, 603–616.e605 (2020).
18. Yamaguchi, N. et al. Chromatin-mediated feed-forward auxin biosynthesis in floral meristem determinacy. *Nat. Commun.* **9**, 5290 (2018).
19. Eshed Williams, L. Genetics of shoot meristem and shoot regeneration. *Annu. Rev. Genet.* **55**, 661–681 (2021).
20. Heisler, M. G. et al. Patterns of auxin transport and gene expression during primordium development revealed by live imaging of the *Arabidopsis* inflorescence meristem. *Curr. Biol.* **15**, 1899–1911 (2005).
21. Long, J. A., Ohno, C., Smith, Z. R. & Meyerowitz, E. M. TOPLESS regulates apical embryonic fate in *Arabidopsis*. *Science* **312**, 1520–1523 (2006).
22. Causier, B., Ashworth, M., Guo, W. & Davies, B. The *TOPLESS* interactome: a framework for gene repression in *Arabidopsis*. *Plant Physiol.* **158**, 423–438 (2012).
23. Plant, A. R., Larrieu, A. & Causier, B. The vital roles of TOPLESS-mediated transcriptional repression in plants. *N. Phytol.* **231**, 963–973 (2021).
24. Espinosa-Ruiz, A. et al. TOPLESS mediates brassinosteroid control of shoot boundaries and root meristem development in *Arabidopsis thaliana*. *Development* **144**, 1619–1628 (2017).
25. Goldberg, A. L. Nobel committee tags ubiquitin for distinction. *Neuron* **45**, 339–344 (2005).
26. Bartel, D. P. MicroRNAs: genomics, biogenesis, mechanism, and function. *Cell* **116**, 281–297 (2004).
27. Borges, F. & Martienssen, R. A. The expanding world of small RNAs in plants. *Nat. Rev. Mol. Cell Biol.* **16**, 727–741 (2015).
28. Chen, X. A microRNA as a translational repressor of *APETALA2* in *Arabidopsis* flower development. *Science* **303**, 2022–2025 (2004).
29. Ramachandran, V. & Chen, X. Small RNA metabolism in *Arabidopsis*. *Trends Plant Sci.* **13**, 368–374 (2008).
30. Voinnet, O. Origin, biogenesis, and activity of plant microRNAs. *Cell* **136**, 669–687 (2009).
31. D'Ario, M., Griffiths-Jones, S. & Kim, M. Small RNAs: big impact on plant development. *Trends Plant Sci.* **22**, 1056–1068 (2017).
32. Song, X., Li, Y., Cao, X. & Qi, Y. MicroRNAs and their regulatory roles in plant-environment interactions. *Annu. Rev. Plant Biol.* **70**, 489–525 (2019).
33. Brodersen, P. & Voinnet, O. Revisiting the principles of microRNA target recognition and mode of action. *Nat. Rev. Mol. Cell Biol.* **10**, 141–148 (2009).
34. Liu, Q. et al. The *ARGONAUTE10* gene modulates shoot apical meristem maintenance and establishment of leaf polarity by repressing miR165/166 in *Arabidopsis*. *Plant J.* **58**, 27–40 (2009).
35. Zhu, H. et al. *Arabidopsis* Argonaute10 specifically sequesters miR166/165 to regulate shoot apical meristem development. *Cell* **145**, 242–256 (2011).
36. Adai, A. et al. Computational prediction of miRNAs in *Arabidopsis thaliana*. *Genome Res.* **15**, 78–91 (2005).
37. Mazhar, M. W. et al. Sequence, secondary structure, and phylogenetic conservation of microRNAs in *Arabidopsis thaliana*. *Bioinform. Biol. Insights* **16**, 11779322221142116 (2022).

38. Song, J. B. et al. miR394 and *LCR* are involved in *Arabidopsis* salt and drought stress responses in an abscisic acid-dependent manner. *BMC Plant Biol.* **13**, 210 (2013).
39. Knauer, S. et al. A protodermal miR394 signal defines a region of stem cell competence in the *Arabidopsis* shoot meristem. *Dev. Cell* **24**, 125–132 (2013).
40. Song, J. B. et al. Altered fruit and seed development of transgenic rapeseed (*Brassica napus*) over-expressing microRNA394. *PLoS ONE* **10**, e0125427 (2015).
41. Litholdo, C. G. Jr. et al. Proteomic identification of putative microRNA394 target genes in *Arabidopsis thaliana* identifies major latex protein family members critical for normal development. *Mol. Cell Proteom.* **15**, 2033–2047 (2016).
42. Lu, L. et al. miR394 enhances WUSCHEL-induced somatic embryogenesis in *Arabidopsis thaliana*. *N. Phytol.* **238**, 1059–1072 (2023).
43. Song, J. B., Huang, S. Q., Dalmay, T. & Yang, Z. M. Regulation of Leaf morphology by microRNA394 and its target *LEAF CURLING RESPONSIVENESS*. *Plant. Cell. Physiol.* **53**, 1283–1294 (2012).
44. Kumar, A. et al. Identification and co-evolution pattern of stem cell regulator miR394s and their targets among diverse plant species. *BMC Evol. Biol.* **19**, 55 (2019).
45. Qu, L., Lin, L. B. & Xue, H. W. Rice miR394 suppresses leaf inclination through targeting an F-box gene, *LEAF INCLINATION 4*. *J. Integr. Plant Biol.* **61**, 406–416 (2019).
46. Du, F. et al. Dose-dependent AGO1-Mediated Inhibition of the miRNA165/166 pathway modulates stem cell maintenance in *Arabidopsis* shoot apical meristem. *Plant Commun.* **1**, 100002 (2020).
47. Gagne, J. M., Downes, B. P., Shiu, S. H., Durski, A. M. & Vierstra, R. D. The F-box subunit of the SCF E3 complex is encoded by a diverse superfamily of genes in *Arabidopsis*. *Proc. Natl Acad. Sci. USA* **99**, 11519–11524 (2002).
48. Hindley, C. J., McDowell, G. S., Wise, H. & Philpott, A. Regulation of cell fate determination by Skp1-Cullin1-F-box (SCF) E3 ubiquitin ligases. *Int. J. Dev. Biol.* **55**, 249–260 (2011).
49. Yan, J. et al. The *Arabidopsis* F-box protein CORONATINE INSENSITIVE1 is stabilized by SCFCOI1 and degraded via the 26S proteasome pathway. *Plant Cell* **25**, 486–498 (2013).
50. Landrein, B. et al. Mechanical stress contributes to the expression of the *STM* homeobox gene in *Arabidopsis* shoot meristems. *Elife* **4**, e07811 (2015).
51. Kieffer, M. et al. Analysis of the transcription factor *WUSCHEL* and its functional homologue in *Antirrhinum* reveals a potential mechanism for their roles in meristem maintenance. *Plant Cell* **18**, 560–573 (2006).
52. Di Giacomo, E., Serino, G. & Frugis, G. Emerging role of the ubiquitin proteasome system in the control of shoot apical meristem function. *J. Integr. Plant. Biol.* **55**, 7–20 (2013).
53. Wang, L., Kim, J. & Somers, D. E. Transcriptional corepressor *TOPLESS* complexes with pseudoresponse regulator proteins and histone deacetylases to regulate circadian transcription. *Proc. Natl Acad. Sci. USA* **110**, 761–766 (2013).
54. Smith, Z. R. & Long, J. A. Control of *Arabidopsis* apical-basal embryo polarity by antagonistic transcription factors. *Nature* **464**, 423–426 (2010).
55. Zhu, Z. et al. *Arabidopsis* resistance protein SNC1 activates immune responses through association with a transcriptional corepressor. *Proc. Natl Acad. Sci. USA* **107**, 13960–13965 (2010).
56. Niu, D. et al. SIZ1-mediated SUMOylation of TPR1 suppresses plant immunity in *Arabidopsis*. *Mol. Plant* **12**, 215–228 (2019).
57. Wenkel, S., Emery, J., Hou, B. H., Evans, M. M. & Barton, M. K. A feedback regulatory module formed by *LITTLE ZIPPER* and *HD-ZIPIII* genes. *Plant Cell* **19**, 3379–3390 (2007).
58. Gallois, J. L., Woodward, C., Reddy, G. V. & Sablowski, R. Combined SHOOT MERISTEMLESS and WUSCHEL trigger ectopic organogenesis in *Arabidopsis*. *Development* **129**, 3207–3217 (2002).
59. Xing, H. L. et al. A CRISPR/Cas9 toolkit for multiplex genome editing in plants. *BMC Plant Biol.* **14**, 327 (2014).
60. Li, S. et al. Biogenesis of phased siRNAs on membrane-bound polysomes in *Arabidopsis*. *Elife* **5**, e22750 (2016).
61. Kim, D., Paggi, J. M., Park, C., Bennett, C. & Salzberg, S. L. Graph-based genome alignment and genotyping with HISAT2 and HISAT-genotype. *Nat. Biotechnol.* **37**, 907–915 (2019).
62. Love, M. I., Huber, W. & Anders, S. Moderated estimation of fold change and dispersion for RNA-seq data with DESeq2. *Genome Biol.* **15**, 550 (2014).
63. Yeung, K. Y., Haynor, D. R. & Ruzzo, W. L. Validating clustering for gene expression data. *Bioinformatics* **17**, 309–318 (2001).
64. Gu, Z., Eils, R. & Schlesner, M. Complex heatmaps reveal patterns and correlations in multidimensional genomic data. *Bioinformatics* **32**, 2847–2849 (2016).
65. Wu, T. et al. ClusterProfiler 4.0: a universal enrichment tool for interpreting omics data. *Innovation* **2**, 100141 (2021).
66. Becker, R. A., Chambers, J. M. & Wilks, A. R. The new S language: a programming environment for data analysis and graphics. (2018).
67. Martin, M. Cutadapt removes adapter sequences from high-throughput sequencing reads. *Embnet. J.* **17**, 10–12 (2011).
68. Liao, Y., Smyth, G. K. & Shi, W. FeatureCounts: an efficient general purpose program for assigning sequence reads to genomic features. *Bioinformatics* **30**, 923–930 (2014).
69. Robinson, M. D., McCarthy, D. J. & Smyth, G. K. EdgeR: a bioconductor package for differential expression analysis of digital gene expression data. *Bioinformatics* **26**, 139–140 (2010).
70. Shi, B., Wang, H. & Jiao, Y. Live imaging of *Arabidopsis* axillary meristems. *Methods Mol. Biol.* **2094**, 59–65 (2020).
71. Fischer, A. H., Jacobson, K. A., Rose, J. & Zeller, R. Paraffin embedding tissue samples for sectioning. *Csh. Protoc.* **2008**, pdb.prot4989 (2008).
72. Cui, R. et al. Functional conservation and diversification of class E floral homeotic genes in rice (*Oryza sativa*). *Plant J.* **61**, 767–781 (2010).
73. Kidner, C. & Timmermans, M. In situ hybridization as a tool to study the role of microRNAs in plant development. *Methods Mol. Biol.* **342**, 159–179 (2006).

Acknowledgements

We would like to thank Prof. Xuemei Chen (Peking University) for miR394 genetic materials, helpful discussions and critical reading for the manuscript. We would like to thank Prof. Lei Wang (Institute of Botany) for the seeds of *tpl-1* and *pTPL::TPL*, and Prof. Jingbo Jin (Institute of Botany) for the seeds of *tpl*, *tpr1*, *tpr2*, *tpr3*, *tpr4* and *tpl tpr1 tpr4* mutants. We also thank Dr. Fengqin Dong, Dr. Jingquan Li, Dr. Xiuping Xu and Dr. Zhuang Lu (Institute of Botany) for technical assistance. This work was supported by the National Key Research and Development Program of China (2023YFF1001301), the Strategic Priority Research Program of the Chinese Academy of Sciences (grant no. XDA24010106-2) to C.Z.

Author contributions

C.Z. and L.L. designed the research. L.L. performed most of the experiments and analyzed the data. B.H. analyzed the RNA seq and sRNA seq data. S.G. performed the northern blot experiments. Z.X. and T.W. conducted some of the experiments and provided suggestions for RNA in situ hybridization and protein experiments. C.Z. and L.L. wrote the manuscript.

Competing interests

The authors declare no competing interests.

Additional information

Supplementary information The online version contains supplementary material available at https://doi.org/10.1038/s41467-024-54494-6.

Correspondence and requests for materials should be addressed to Cui Zhang.

Peer review information *Nature Communications* thanks Raffaele Dello Ioio, Giovanna Frugis and the other, anonymous, reviewer(s) for their contribution to the peer review of this work. A peer review file is available.